Attenuating NKG2D stimulation reshapes intratumoral NK cell functional state to enhance persistence and anti-tumor efficacy

Sizhe Liu[1], Ryan Joseph Brown[2], Payal Dhar[1,†], Geetha Priyanka Yerradoddi[3], Tyler Aaron Smith[1], Bin Zhang[4], Deyu Fang[2], Congcong He[5], David VanderWeele[4], Masha Kocherginsky[6], Arabela Grigorescu[7], Seth M. Pollack[4], Qingshu Meng[1], Qi Cao[1], Karla Guerra[1], Weiguo Cui[2], Jennifer D. Wu[1*]

[1]Department of Urology, Feinberg School of Medicine, Northwestern University, Chicago, IL 60611, USA

[2]Department of Pathology, Feinberg School of Medicine, Northwestern University, Chicago, IL 60611, USA

[3]Center for Research Informatics, The University of Chicago, Chicago, IL60611, USA

[4]Department of Hematology and Oncology, Feinberg School of Medicine, Northwestern University, Chicago, IL 60611, USA

[5]Department of Cell and Developmental Biology, Feinberg School of Medicine, Northwestern University, Chicago, IL 60611, USA

[6]Department of Preventive Medicine, Feinberg School of Medicine, Northwestern University, Chicago, IL 60611, USA

[7]Keck Biophysics Facility, Lurie Cancer Center, Northwestern University, Evanston, IL 60208, USA

[†]Current address: Bristol Myers Squibb, South San Francisco, CA 94080, USA.

Running Title: Attenuating NKG2D stimulation enhances NK cell efficacy

Keywords: NKG2D, partial agonist antibody, NK cell, stemness, persistence

Abstract

NK cell-based therapies for solid tumors are limited by poor persistence and progressive functional impairment. Here, we investigated how the strength of NKG2D stimulation shapes NK cell fate and therapeutic efficacy. Using B10G5, a MICA/B-targeting partial agonist antibody that attenuates NKG2D stimulation, we show that reduced NKG2D stimulation reshapes the intratumoral NK cell compartment by enriching $EOMES^{hi}TCF1^{hi}$ stem-like NK (stemNK) cell pool, preserving functional diversity, and limiting mitochondrial oxidative stress and exhaustion induced by chronic sMIC/MIC exposure. Mechanistically, we identified the H3K27me3 demethylase KDM6B as a conserved regulator of NK cell stemness whose enzymatic activity is required to maintain the intratumoral stemNK cell pool. Conversely, strong NKG2D stimulation induced mitochondrial ROS accumulation and upregulated the inhibitory receptor LAG3 on NK cells. Attenuated NKG2D stimulation on human NK cells increased KDM6B expression and reduced repressive H3K27me3 mark at the *TCF7* locus. Importantly, attenuated NKG2D stimulation during ex vivo expansion enhanced human NK cell in vivo persistence and antitumor efficacy following adoptive transfer. Together, these findings establish NKG2D stimulation strength as a key determinant of NK cell fate and function in solid tumors and identify a translatable strategy to improve NK cell-based immunotherapy for solid tumors.

Introduction

Natural killer (NK) cells play a critical role in tumor immune surveillance through direct cytotoxicity and by producing cytokines and chemokines to orchestrate broader anti-tumor responses. These properties have driven the development of NK cell-based therapies, including NK cell engagers and chimeric antigen receptor (CAR)-NK cells. Despite encouraging clinical activity observed in hematological malignancies (1, 2), therapeutic efficacy in solid tumors remains limited by poor NK cell persistence and progressive loss of function within the tumor microenvironment (TME) (3). Strategies to overcome these limitations are needed.

NKG2D is a major activating receptor constitutively expressed by all human NK cells. Among its ligands, the major histocompatibility complex I chain-related family molecules MICA and MICB (collectively termed MIC) are broadly expressed by human solid tumors and absent in normal tissues (4, 5). Induced MIC expression enables NKG2D-expressing lymphocytes to recognize and limit stressed or transformed cells during early tumorigenesis (6-8). The MIC molecule consists of the $\alpha1\alpha2$ ectodomains that engage NKG2D and an $\alpha3$ domain that facilitates proteolytic shedding (9-11). Tumor shedding of soluble MIC (sMIC) is a prominent immune evasion mechanism utilized by human malignant tumors (4, 12-14). In cancer patients, elevated levels of serum sMIC were associated with impaired NK cell function, reduced functional NK cell numbers, metastatic diseases, and poor clinical outcome (15-18). Conversely, naturally occurring anti-sMIC/MIC antibodies have been associated with enhanced NK cell function and better immunotherapeutic responses in cancer patients (19, 20). These findings underscore the importance of the MIC-NKG2D axis in regulating NK cell anti-tumor immunity. How the strength of NKG2D stimulation influences NK cell fate, persistence, and functional state within solid tumors remains poorly understood.

The biological consequence of NKG2D engagement depends on the context of stimulation. Acute engagement of NKG2D by tumor cell surface ligands promotes NK cell activation and cytotoxicity (6, 21), whereas sustained engagement of NKG2D by either membrane-bound or soluble ligands, can induce NK cell dysfunction (22-25). Despite this distinction, many therapeutic strategies seek to maximize NKG2D engagement or signaling to improve NK cell-based therapeutic efficacy. The clinical outcome remains unsatisfactory.

We previously described a unique class of sMIC/MIC-targeting antibody B10G5 that restores NK cell homeostatic renewal and reinvigorates NK cell function in pre-clinical solid tumor model (17, 26). Here, we investigated the underlying biological mechanism of how B10G5 enables NK cell persistence. We show that B10G5 attenuates MIC binding to NKG2D and utilize this system to investigate how NKG2D stimulation strength regulates NK cell state and function. We find that attenuated NKG2D stimulation enriches an $EOMES^{hi}TCF^{hi}$ stem-like NK cell population, preserves NK cell functional diversity, and limits oxidative stress and exhaustion associated with chronic MIC exposure. We further identify KDM6B as an epigenetic regulator of NK cell stemness. Finally, we demonstrate that attenuating NKG2D stimulation during ex vivo expansion improves NK cell in vivo persistence and antitumor efficacy. These findings identify the strength of NKG2D stimulation as a regulator of NK cell fate and provide a translational concept to improve the durability and efficacy of NK cell-based therapy for solid tumors.

Results

Attenuating NKG2D stimulation enriches intra-tumoral EOMES^{hi}TCF1^{hi} stemNK cells and preserves NK cell functional diversity.

Because mice lack MIC gene (27, 28), we had previously established an engineered bi-transgenic TRAMP/MICB mouse model that recapitulated the MIC/NKG2D biology in human MIC$^+$ solid tumors (17). We had also shown that clearance of tumor-derived sMIC with a murine antibody B10G5 significantly enriched functional tumoral NK cells (26), a finding validated across multiple syngeneic sMIC$^+$ models (26, 29, 30).

To understand how B10G5 therapy shapes NK cell fate and function, we performed scRNA-seq of tumor-infiltrating CD45$^+$ cells from pooled TRAMP/MICB tumors with or without B10G5 treatment (Figure 1A). After immune cell annotation, NK cells were identified by low *Cd3d/e* expression and enrichment for *Klrb1c* and *Ncr1* (Supplemental Figure 1, A and B). Sub-clustering revealed three intratumoral NK cell subsets (C0-2) (Figure 1B, Supplemental Table S1). Two of the sub-clusters (C0, C1) represented two distinct conventional effector NK cell subsets, tissue-resident NK cells and the cytotoxic NK cells . C1 represented cytotoxic NK cells (cytoNK), marked by gene expression signature of cytotoxic granule molecules (*Prf1, Gzma)*, transcription factors supporting NK cell activation and function (*Irf8, Klf2),* and the terminal differentiation marker (*Klrg1*) (Figure 1C). C0 represents tissue-resident NK cells (trNK), marked by gene expression signature of the common tissue residency markers (*Cxcr6, Itga1, Itgae* and *Rgs1*) and the immuno-modulatory chemokine *(Xcl1)* (Figure 1C, Supplemental Figure 1C).

A unique NK cell sub-cluster (C2) was markedly enriched in B10G5-treated tumors compared with untreated tumors (30.0% vs. 6.1%) (Figure 1, D and E). The C2 subset was defined by a gene expression signature associated with stemness and memory in lymphocytes, including

Tcf7, Eomes, Sell, Myb, and *Satb1* (31-34) (Figure 1C and Supplemental Figure 1D). These stemNK cells (C2) exhibited lower expression of cytotoxic molecules (*Prf1, Gzma/b*) and *Ifng* than cytoNK cells (C1) and lower expression of immuno-modulatory chemokines (*Ccl5, Xcl1)* than trNK cells (C0) (Supplemental Figure 1C), indicating that stemNK cells are not primarily an effector population. Notably, TCF1 (*Tcf7)* expression has been associated with NK cell subsets that function as progenitors capable of replenishing short-lived terminally differentiated effector NK cells (35, 36). Slingshot trajectory inference analysis indicated that stemNK cells may differentiate into either cytoNK or trNK cells (Supplemental Figure 2). Thus, stemNK cells may function as a progenitor reservoir that sustains effector NK-cell diversity and persistent antitumor responses.

We validated the three intratumoral NK-cell subsets by flow cytometry using scRNA-seq-defined markers (Figure 1F): $CD49a^{+}CXCR6^{+}$ for trNK cells, $EOMES^{hi}TCF1^{hi}$ for stemNK cells, and $CXCR6^{-}Perforin^{hi}$ for cytoNK cells (Figure 1G, Supplemental Figure 3). Perforin, encoded by *Prf1*, was selected as the primary cytoNK marker because it is essential for cytotoxic granule-mediated killing and granzyme delivery (37, 38). Consistent with the scRNA-seq findings, B10G5 treatment increased overall NK cells infiltration in TRAMP/MICB tumors, accompanied by a significant enrichment of $EOMES^{hi}TCF1^{hi}$ stemNK cell subset (Figures 1H). These $TCF1^{hi}$ stemNK cells also expressed high levels of EOMES, a transcription factor associated with in vivo persistence of cytokine-induced human memory-like NK cells (39, 40). B10G5 treatment also increased intratumoral cytoNK cell abundance (Figures 1H). Among $Perforin^{hi}$ cytoNK cells, B10G5 treatment did not alter the frequency of granzyme B^{+} cells but significantly increased the frequency of granzyme A^{+} cells (Figure 1, I and J), suggesting broader cytotoxic potential through caspase-independent granzyme A pathways distinct from granzyme B (41). Together, these data

demonstrate that B10G5 treatment enriches intra-tumoral EOMES^{hi}TCF1^{hi} stemNK cells while sustaining and enhancing the functional diversity of effector cells.

To further define how B10G5 treatment shapes intratumoral NK cell function and diversity, we examined its effect on sMIC/MIC engagement with NKG2D. Biolayer interferometry (BLI), showed that pre-formed B10G5/sMIC complexes bound to NKG2D with lower affinity than sMIC alone (Supplemental Figure 4A). Because sMIC and cell surface MIC share the same NKG2D-binding $\alpha1\alpha2$ domain, these findings suggest that B10G5 may similarly attenuate cell surface MIC binding to NKG2D, an effect supported by cell-based assays. In MIC^{+} K562 cells, B10G5 pre-incubation reduced recombinant NKG2D-Fc binding, as measured with flow cytometry, with inhibition detectable at 100 ng/ and plateauing near 1 μg/mL (Supplemental Figure 4B). Similarly, pre-formed B10G5/sMIC complexes at the molar ratios of 0.3 or greater showed reduced binding to NKG2D on primary human NK cells compared with MIC alone (Supplemental Figure 4C). Together, these biophysical and cell-based data demonstrate that B10G5 attenuates, rather than fully blocks, sMIC/MIC engagement with NKG2D, providing a mechanistic basis for modulating NKG2D signaling.

Attenuating NKG2D stimulation mitigates LAG3 and NKG2A expression of tumor resident NK cells

In addition to activating receptors, NK cell activity is regulated by co-inhibitory receptors, including PD-1, TIGIT, LAG3, and NKG2A, which have been implicated in NK cell exhaustion (42). Analysis of our scRNA-seq dataset revealed distinct expression patterns of *Lag3 and Klrc1,* encoding LAG3 and NKG2A respectively. *Lag3* expression was largely restricted to trNK cells (C0), whereas *Krlc1* was expressed across all NK cell subsets (Supplemental Figures 5, A and B).

In contrast, *Pdcd1* and *Tigit*, encoding PD-1 and TIGIT, respectively, were not readily detected at the transcript level (Supplemental Figure 5, A and B) and thus were not pursued further. These expression patterns were further confirmed at the protein level (Supplement Figure 5C). Although the frequency of NKG2A$^+$ cells was significantly higher in trNK cells than in non-trNK cells, NKG2A expression on a per-cell basis was not significantly different between these populations (Supplemental Figure 5D). B10G5 treatment significantly reduced the frequency of LAG3$^+$trNK and NKG2A$^+$ trNK cell populations (Figures 2, A-D) but did not significantly alter on their per cell expression levels as measured by gMFI although a trend towards reduced per-cell LAG3 expression was observed (Supplement Figures 5E). B10G5 treatment did not significantly alter NKG2A expression on non-trNK cells (Figure 5F). These data suggest that B10G5 treatment primarily reduces the abundance of LAG3$^+$ and NKG2A$^+$ trNK cells.

We also examined the expression of KLRG1, a receptor associated with NK cell terminal differentiation (43). At the transcript level, *Klrg1* was exclusively expressed on the cytoNK cell subset C1 (Supplemental Figure 5A-B, Figure 1C). B10G5 treatment did not significantly alter *Klrg1* expression on cytoNK cells (Supplemental Figure 5G), which was validated at the protein level with flow cytometry (Supplemental Figure 5H, 5I). Notably, tumoral KLRG1$^+$ cytoNK cells exhibited higher protein expression of perforin and granzyme A than KLRG1$^-$ cytoNK cells (Supplemental Figure 5J), indicating that KLRG1 marks a highly cytotoxic effector NK cell population in our model.

Attenuating NKG2D stimulation reduces mitochondrial ROS of tumoral NK cells

Given that mitochondrial fitness governs NK cell function (44, 45), we next examined whether chronic sMIC/MIC exposure disrupts mitochondrial homeostasis in tumoral NK cells.

Pathway enrichment analysis revealed a marked dysregulation of mitochondrial and oxidative stress-related gene programs in NK cells from untreated tumors, including genes involved in the respiratory electron transport chain (ETC), NRF2 (*Nfe2l2*) signaling and cellular stress response pathways (Figure 2E). The ETC is central to ATP production but is also a major source of reactive oxygen species (ROS) (46). In the hypoxic tumor microenvironment, ETC inefficiency can drive mitochondrial ROS accumulation and activation of oxidative stress response pathways (46-48).

To quantify oxidative stress at the single-cell level, we employed Seurat's AddModuleScore function to calculate module scores based on the average expression of gene set associated with excessive oxidative stress and cellular damage (Figure 2F). This gene set included genes encoding for antioxidant enzymes (*Prdx5, Prdx6),* Nrf2-activated proteasome *(Psma1, Psma4, Psma7),* and stress- and apoptosis-related molecules (*Txnip, Gadd45g, Dapk2*) (Supplemental Figure 6A). B10G5 treatment reduced the oxidative stress module score in both trNK and cytoNK effector subsets (Figure 2F), suggesting that chronic sMIC/MIC stimulation broadly comprises effector NK cell fitness.

We next validated these transcriptional findings by flow cytometry. Assessment of mitochondrial ROS (mtROS) with MitoSox and mitochondrial membrane potential with MitoTracker Deep Red-to-Green ratio confirmed that chronic sMIC/MIC exposure was associated with significantly increased mtROS accumulation and impaired mitochondrial potential in tumoral NK cells. Notably, B10G5 treatment markedly decreased the frequency of $MitoSox^+$ NK cells and restored mitochondrial potential (Figure 2, G and H). Moreover, the frequency of $MitoSox^+$ NK cells positively correlated with the expression of the exhaustion marker LAG3 (Figure 2I), linking mitochondrial oxidative stress to NK cell dysfunction. Consistent with these findings, NK cells NK cells from sMIC-overexpressing TRAMP-C2-sMICB syngeneic tumors showed increased

mtROS accumulation, further confirming chronic sMIC-mediated NKG2D stimulation promoting mitochondrial oxidative stress (Supplemental Figure 6, B and C). In this model, B10G5 targeting sMIC/MIC significantly reduced the DNA damage marker phospho-H2AX in tumoral NK cells, suggesting that mtROS accumulation may contribute to genotoxic stress (49) (Supplemental Figure 6D). Together, these data indicate that sMIC in the TME drives mitochondrial oxidative stress and NK cell dysfunction, whereas attenuation of NKG2D stimulation with B10G5 restores NK cell mitochondrial fitness by limiting mtROS accumulation.

KDM6B is a candidate regulator of NK cell stemness

Given the importance of TCF1^{hi} stemNK cells in sustaining NK cell persistence and durable anti-tumor function (50), we sought to define molecular mechanisms underlying B10G5-mediated enrichment in stemNK cell reservoir. To this end, we identified genes that were enriched in stemNK cells and upregulated following B10G5 treatment (Figure 3A). The overlapping genes were significantly enriched in pathways related to chromatin remodeling and histone modification (Supplemental Table S2, Figure 3B). These included genes encoding components of chromatin remodeling complexes (*Chd3/4; Chd7*), chromatin organizers (*Satb1, Myb*), histone modifiers (*Kdm6b, Kdm2b, Ash1l*), and histone chaperones or chromatin-associated factors (*Npm1, Emsy*) (Figure 3C).

Because stem-like cell states require dynamic epigenetic regulation (34, 51, 52), we focused on *Kdm6b*, which encodes the H3K27me2/3 demethylase KDM6B, a regulator of active transcription and stem cell maintenance (53, 54). Pseudotime analysis of scRNA-seq trajectories showed that *Kdm6b* expression was highest in stemNK cells and progressively decreased as cells transitioned toward effector phenotypes (Figure 3, D and E), implicating KDM6B in maintenance

of NK cell stemness. To identify putative KDM6B target genes, we leveraged ChIP-Atlas-curated KDM6B ChIP-seq datasets (55) and intersected predicted targets with differentially expressed genes between stemNK and trNK or cytoNK subsets in B10G5-treated tumors (Figure 3F-G). Notably, *Tcf7* was identified as a candidate KDM6B target, with KDM6B binding sites proximal to mouse *Tcf7* promoter (Supplemental Figure 7A). KDM6B binding appeared to coincide with H3K27me3 modification at the promoter region (Supplemental Figure 7A), suggesting potential epigenetic maintenance of *Tcf7* expression in stemNK cells. Additional putative KDM6B targets included transcription factors (*Eomes, Klf2, Rbpj*), chemokine receptors (*Cxcr4, Sell*), and genes involved in adhesion, metabolism, and signaling (*Emb, Pde2a, Sh2d1a, Socs3, Pmepa1*) (Figure 3, F and G). These findings support a coordinated KDM6B-regulated gene network sustaining stemNK identity.

To assess relevance in human cancer, we analyzed a pan-cancer tumoral NK cell scRNA-seq dataset (GSE212890) (56). Three conserved NK subsets, stemNK cell *($TCF7^+$)*, cytoNK cell ($PRF1^+$, $FCGR3A^+$), and trNK cell ($CXCR6^+$, $ITGAE^+$) were identified, mirroring mouse datasets (Figure 3, H and I and Supplemental Figure 7B). Thirty-four stemNK cell-associated marker genes were shared between mouse and human (Supplemental Figure 7C). Genes encoding for three epigenetic modifiers, SATB1, KDM6B, and CHD4, which were enriched in mouse stemNK cell subsets were also highly expressed in the human stemNK cell subset (Figure 3J), with the enrichment for KDM6B showing the most consistent enrichment across species. Collectively, these data identify KDM6B as a conserved candidate epigenetic regulator associated with maintenance of the stemNK cell pool in tumors.

KDM6B demethylase activity is required for maintaining tumoral stemNK cell pool

In addition to its demethylase activity, KDM6B has been reported to regulate gene expression through interactions with chromatin remodeling complexes and transcriptional machinery (57, 58). Our scRNA-seq analyses of both mouse and human stemNK cells (Figure 3C, 3J), together with co-localization of KDM6B occupancy and H3K27me3 marks around the *Tcf7* gene locus (Supplemental Figure 7A), suggested that KDM6B demethylase activity may directly contribute to stemNK cells maintenance. We therefore tested whether KDM6B enzymatic activity is required for B10G5-mediated enrichment of the stemNK cell pool.

We treated syngeneic TRAMP-C2-MICB tumor-bearing mice with B10G5, with or without co-administering the KDM6B demethylase inhibitor GSK-J4 (Figure 4A). Consistent with our findings in the TRAMP/MICB transgenic autochthonous model, B10G5 therapy significantly inhibited tumor growth and enriched total NK cell and $EOMES^{hi}TCF1^{hi}$ stemNK cell pool in tumors (Figure 4, B and C, Supplemental Figure 8). StemNK cell enrichment was accompanied by increased KDM6B expression following B10G5 treatment (Figure 4, D and E), with KDM6B level significantly higher in $EOMES^{hi}TCF1^{hi}$ stemNK cells than in $EOMES^{lo}/TCF1^{lo}$ NK cell subsets (Figure 4F). Co-administering GSK-J4 with B10G5 markedly attenuated these effects, resulting in a significant reduction of the intratumoral stemNK pool (Figure 4, B and C). These findings indicated that KDM6B demethylase activity is required for maintaining stemNK cells in tumors. Notably, GSK-J4 treatment also significantly reduced KDM6B expression in stemNK cells (Figure 4D), suggesting a potential auto-regulatory mechanism. Supporting this possibility, analysis of publicly available KDM6B ChIP-seq datasets revealed KDM6B binding sites within the *Kdm6b* promoter region in both mouse and human cells (Supplemental Figure 9, A and B).

To examine whether tumor burden was associated with the observed changs in stemNK cells, we performed Pearson correlation analyses between the final tumor volume (mm^3) and the

247 percentage of stemNK cells or KDM6B expression (gMFI) of stemNK population. Tumor volume
248 was negatively correlated with stemNK frequency and KDM6B expression (Figure 4, G and H).
249 These findings support an association between B10G5-mediated stemNK cell enrichment and
250 improved tumor control.
251
252 **Attenuating NKG2D stimulation upregulates KDM6B and TCF1 expression in human NK**
253 **cells**
254 Based on the scRNA-seq analyses identifying the similarity between human and mouse
255 stemNK cells (Figure 3, H and I), we examined whether a $TCF1^{hi}$ NK cell subset could be detected
256 in bulk human PBMCs. Human peripheral blood NK cells contain distinct $TCF1^{hi}$ and $TCF1^{lo}$
257 subsets (Figure 5A). Consistent with the mouse data, $TCF1^{hi}$ NK cells expressed higher levels of
258 EOMES (Supplemental Figure 10A), a transcription factor required for NK cell functional
259 persistence in vivo (59, 60). Upon 4h co-culture of PBMCs with K562 target cells at a E:T ratio of
260 5:1, $TCF1^{hi}$ NK cells showed comparable IFNγ production and degranulation to $TCF1^{lo}$ NK cells
261 but consistently lower expression of the cytotoxic molecule Perforin than $TCF1^{lo}$ NK cells across
262 all tested donors (Supplemental Figure 10, B-D). This $Perforin^{lo}$ phenotype mirrored mouse
263 $TCF1^{hi}$ stemNK (Figure 1F), supporting the concept that $TCF1^{hi}$ stemNK cells are not primarily
264 cytotoxic effectors.
265 Given the role of TCF1 in NK cell persistence (50), we assessed whether sMIC and
266 B10G5/sMIC stimulation differentially modulates TCF1 expression in NK cells using healthy
267 donor PBMCs. Stimulation with pre-formed B10G5/sMIC complex significantly increased the
268 frequency of $TCF1^{hi}$ NK cells compared with sMIC alone (Figure 5B), suggesting that
269 sequestering sMIC by B10G5 may enrich stemNK cells in humans.

Consistent with findings from mouse and human scRNA-seq analyses shown in Figure 3C and 3J, peripheral blood TCF1^{hi} human NK cells expressed significantly higher levels of KDM6B than TCF1^{lo} NK cells (Figure 5C), suggesting a conserved association between KDM6B and NK cell stemness. To further assess whether sMIC and B10G5/sMIC stimulation differentially regulates KDM6B and human NK cell stemness, we cultured primary human NK cells in the presence of recombinant sMIC or pre-formed B10G5/sMIC complex. Acute sMIC stimulation for 6h increased *KDM6B* transcript levels (Supplemental Figure 11, A and B), whereas prolonged stimulation from 18h to 5 days induced higher *KDM6B* expression with sMIC/B10G5 stimulation than sMIC alone, reaching an approximate 1.2-fold increase by day 5 (Supplemental Figure 11, C-E). KDM6B is known to function epigenetically in the nucleus (61, 62). We thus assessed nuclear KDM6B expression. After 5 days of stimulation, sMICB/B10G5 complex induced a significantly greater nuclear accumulation of KDM6B than sMICB alone (Figure 5D-E). Together, these findings indicate that B10G5-mediated sequestration of sMIC enhances KDM6B expression and nuclear localization with a concomitant increase in TCF1 expression in human NK cells, supporting a conserved role for the KDM6B-TCF1 axis in stem-like NK cell maintenance.

Attenuating NKG2D stimulation during ex vivo expansion enhances NK cell in vivo persistence and anti-tumor efficacy

Irradiated K562-CI9-mIL21 feeder cells are widely used to expand NK cells from PBMCs for clinical investigations (63, 64); however, limited in vivo persistence of infused NK cells remains a major challenge (3, 65). Given the malignant origin of K562 cells (66), we investigated whether the K562-CI9-mIL21 feeder cells express and shed MIC ligands that could adversely affect NK cell fitness during expansion. Flow cytometry revealed robust surface MIC expression

on K562-CI9-mIL21 cells (Supplemental Figure 12A). Irradiation only modestly reduced surface MIC expression (<15%), but markedly increased soluble MIC shedding by the feeder cells on a per-cell basis, with preferential accumulation of sMICB in culture supernatants (Supplemental Figure 12, A-D). These findings indicate a chronic sMIC/MIC exposure during ex vivo NK cell expansion.

To determine whether the persistent sMIC/MIC exposure during expansion compromises NK cell stemness and anti-tumor function, K562-CI9-mIL21 feeder cells were pre-incubated with B10G5 to attenuate sMIC/MIC-mediated chronic stimulation; these NK cells were designated as "B10G5-conditioned" NK cells as to "unconditioned" NK cell expanded without B10G5. Immediately following expansion without additional stimulation, we profiled these NK cells using flow cytometry. B10G5 pre-conditioning did not markedly alter surface receptors profiles or cytotoxicity (Supplemental Figures 13 and 14), indicating that B10G5 attenuating sMIC/MIC-mediated NKG2D stimulation did not substantially alter baseline phenotype or immediate effector functions of expanded NK cells.

We next investigated whether B10G5-conditioning ex vivo enhances NK cell persistence and anti-tumor efficacy following adoptive transfer in vivo (Figure 6A). Unconditioned and B10G5-conditioned NK cells were evaluated in NCG mice bearing MIC^{+} PC-3 prostate tumors, either as monotherapy or in combination with Ab-K1, a humanized B10G5 engineered with a human IgG1-Fc to enable antibody-dependent cellular cytotoxicity (ADCC) (Supplemental Figure 15). Unconditioned NK cells failed to control tumor growth, whereas B10G5-conditioned NK cells significantly inhibited tumor growth (Figure 6B). Tumor control was further enhanced by the combination with Ab-K1 (Figure 6C), potentially through continuous in vivo conditioning and AB-K1-mediated ADCC effect. Consistent with improved anti-tumor activity, B10G5-conditioned

NK cells accumulated at a significantly higher level within tumors (Figure 6, D and E) and exhibited an increased frequency of $CD16^{hi}$ subsets (Figure 6, F and G). Conditioned NK cells also had increased expression of the stemness-associated factors KDM6B, TCF1, and EOMES compared with unconditioned NK cells (Figure 6, H and I). Together, these findings indicate that although B10G5-conditioning did not substantially alter NK cell phenotypes ex vivo, it enhanced the ability of adoptively transfer NK cells to persist and maintain stemness-related features in tumors. These data support the concept that limiting chronic MIC/sMIC-mediated NKG2D stimulation during expansion preserves NK cells fitness and provide a potential translatable strategy to improve the persistence and anti-tumor efficacy of adoptively transferred NK cell therapies for solid tumors.

Attenuating NKG2D stimulation reduces repressive H3K27me3 at the *TCF7* locus

To further define how attenuation of NKG2D stimulation by B10G5 modulates TCF1 expression in human NK cells, we investigated whether KDM6B, which is upregulated in response to B10G5, could promote *TCF7* transcription through H3K27me3 demethylation. We first examined ChIP-Atlas-curated human KDM6B ChIP-seq datasets together with publicly available H3K27me3 profiles from human NK cells. KDM6B occupancy overlapped with H3K27me3-enriched regions at the *TCF7* promoter and a predicted upstream enhancer (GH05J134070) (Figure 7A), suggesting that these regulatory regions may be the direct targets of KDM6B-mediated demethylation of H3K27me3.

We next determined whether NKG2D stimulation with sMIC versus B10G5/sMIC complex differentially regulates H3K27me3 at the *TCF7* locus. After primary human NK cells were cultured in the presence of recombinant sMIC or pre-formed B10G5/sMIC complexes for

five days, we quantified H3M27me3 enrichment at the *TCF7* promoter and enhancer regions by CUT&RUN-qPCR. sMIC stimulation increased H3K27me3 enrichment relative to no stimulation control. In contrast, B10G5/sMIC complex stimulation significantly reduced H3K27me3 enrichment compared with sMIC-stimulation, reducing the H3K27me3 enrichment (Figure 7B). Together, our findings support a model in which attenuating NKG2D stimulation with B10G5 promotes KDM6B expression and reduces the repressive H3K27me3 at the *TCF7* regulatory region, thereby establishing an epigenetic state permissive for *TCF7* expression and maintenance of NK stemness in vivo within tumor microenvironment.

Discussion

In this study, we demonstrate that attenuating NKG2D stimulation with a partial agonist antibody B10G5 targeting sMIC/MIC reshapes the intratumoral NK cell compartment by enriching an EOMES^{hi}TCF1^{hi} stemNK cell pool, preserving functional diversity, and limiting oxidative stress and exhaustion otherwise associated with chronic sMIC/MIC exposure. Mechanistically, we identify the histone demethylase KDM6B as a conserved regulator of NK cell stemness and demonstrate that its enzymatic activity is required to sustain the EOMES^{hi}TCF1^{hi} stemNK pool in tumors. We demonstrate that attenuating NKG2D stimulation mitigated mtROS accumulation and prevented the expression of the inhibitory receptor LAG3 on tumoral NK cells, potentially contributing to sustained NK cell function in tumors. Extending these findings to a translational setting, we show that attenuation of NKG2D stimulation during ex vivo NK cell expansion improves subsequent in vivo persistence and antitumor efficacy. Together, these findings reveal a previously unrecognized mechanism by which the strength of NKG2D stimulation governs NK cell fate and function and suggest a viable approach to enhance NK cell-based immunotherapy for solid tumors.

Although NKG2D is a canonical activating receptor on NK cells, the biological consequences of its engagement are highly context dependent. Acute stimulation by membrane-bound ligands promotes NK cell activation, whereas sustained or high-intensity stimulation can impair NK-cell responsiveness, degrade downstream signaling adaptors, and induce cross-tolerance of other activating receptors (6, 22-24). Together, these observations suggest that both strength and duration of NKG2D stimulation shape NK cell functional states and persistence in tumors. Our data support a model in which chronic, strong NKG2D ligand engagement negatively

affects NK cell fate and function, whereas attenuated NKG2D stimulation preserves NK cell fitness and persistence.

Current strategies to mitigate the immunosuppressive effects of soluble MIC largely focus on targeting the α3 domain to inhibit MIC shedding while preserving NKG2D engagement (11, 67-69). Although such approaches effectively stabilize tumor cell surface MIC, their enhancement of NK cell activity may depend largely on Fc-mediated mechanisms (67, 69). Our data raised the possibility that sustained surface MIC stabilization may have context-dependent effects on NK cell fitness, particularly under conditions of prolonged NKG2D engagement by high affinity ligands. Thus, therapies targeting MIC-NKG2D axis should consider not only ligand abundance, but also the strength and duration of NKG2D stimulation within the tumor microenvironment.

B10G5 binds both soluble and membrane-bound MIC; the relative contribution of each source to its therapeutic activity remains to be defined. sMIC can have a profound negative impact on NK cell function and TME (4, 17), although chronic stimulation by either sMIC or membrane MIC can induce NK cell dysfunction (6, 22-24). One possible explanation is that sMIC may continuously engages NKG2D independently of NK-tumor cell contact and productive immune synapse formation., whereas membrane MIC engagement may terminate after tumor cell killing. Thus, complexing sMIC with B10G5 and modulating its interaction with NKG2D may contribute substantially to therapeutic benefit. Future studies should determine how B10G5 differentially modulates soluble versus membrane-bound MIC signaling through NKG2D.

Although this study focuses on NK cells, NKG2D is expressed by $CD8^+$ T cells, γδ T cells, NKT cells, and subsets of innate lymphoid cells (70, 71), where it functions as a co-stimulatory or activating receptor (70). Because B10G5 efficacy depends on both NK and $CD8^+$ T cells (26), B10G5 may also modulate NKG2D signaling in additional immune populations. Defining these

effects and their contribution to therapeutic response will be an important area for future investigation.

Limited persistence remains a major obstacle for NK cell-based therapies for solid tumors (3). Recent studies have identified TCF1^{hi} stemNK cell subsets with enhanced persistence and proliferative potential (50), yet strategies to sustain this state remain limited. To date, STING pathway activation was reported to enrich and sustain TCF1^{hi} NK cell in tumors (50). Here, we show that tuning the strength of NKG2D ligand binding through B10G5 promoted NK cell stemness, characterized by sustained TCF1 and EOMES expression. This stemNK-cell population is distinct from cytokine-induced memory-like (CIML) NK cells (72, 73), which were generated by transient IL-12/15/18 preactivation with enhanced effector response against hematological tumors, in potential association with TCF1 expression (73, 74). The stemNK cells described in this study are relatively quiescent but may sustain the intratumoral NK-cell pool in solid tumor microenvironment by giving rise to effector cytoNK and trNK populations.

We identify KDM6B as a conserved epigenetic regulator of NK cell stemness in mouse and human. KDM6B removes repressive H3K27me2/3 marks to promote transcription but can also act through demethylase-independent mechanisms involving chromatin remodeling complexes, transcriptional machinery, elongation factors, and enhancer formation (57, 75, 76). Its reduced oxygen dependency compared with other H3K27 demethylases suggests that KDM6B may be particularly relevant in hypoxic tumor microenvironments (3, 77). KDM6B function is highly dependent on cell type and developmental stage (53). It maintains HSC self-renewal and restrains differentiation (54), regulates CD8$^+$ T cell effector function and differentiation (78, 79), and can overcome hypoxia-induced CD8$^+$ T cell exhaustion when enforced in tumors (80). In NK cells, however, its role remains poorly defined, with limited in vitro evidence showing that GSK-

J4-mediated inhibition impairs cytokine secretion (81). Our data establishes a requirement for KDM6B demethylase activity in maintaining stemNK cells in tumors, while the contribution of its non-enzymatic functions to NK cell fate remains to be determined.

Lymphocyte exhaustion is characterized by expression of co-inhibitory receptors such as LAG3 and failure to metabolically adapt to the TME (82). We show that chronic sMIC exposure is associated with increased mtROS and LAG3 expression in tumoral NK cells, both of which are attenuated by B10G5. Because metabolic flexibility is critical for sustaining NK cell antitumor function (44) and LAG3 can regulate the balance between glycolysis and mitochondrial respiration in regulatory T cells (83), LAG3 may similarly influence NK cell metabolic adaptation in tumors. LAG3 expression in tumor-infiltrating T cells from prostate cancer patients has also been associated with ATM deficiency and compromised DNA damage repair (84). Our findings link NKG2D ligand engagement strength, oxidative stress, and LAG3 expression, suggesting that combined targeting of the NKG2D and LAG3 axes may provide synergistic therapeutic benefit.

In conclusion, our data supports a model in which the strength and duration of NKG2D stimulation critically influence NK cell fate and function, favoring either persistence and sustained anti-tumor function or progressive functional exhaustion. Our findings challenge the prevailing assumption that maximizing NKG2D stimulation will necessarily improve NK cell therapeutic efficacy. Instead, we demonstrated that attenuating NKG2D ligand stimulation during ex vivo expansion can preserve NK cell stemness, improve in vivo persistence, and enhance anti-tumor efficacy. More broadly, the concept that NKG2D stimulation should be optimized rather maximized may have implications for designing CAR-NK cells, NK cell engagers, and other NK cell-based therapies for solid tumors.

Methods

Sex as a biological variable

Our study exclusively examined male mice for prostate cancer models. It is unknown whether the findings are relevant for female mice.

Cell Lines

TRAMP-C2-sMICB, TRAMP-C2-MICB, PC3 and K562-CI9-mIL21 cells were cultured in RPMI-1640 (Gibco) medium supplemented with 10% heat inactivated FBS (Neuromics), 100U U/mL penicillin and 100 ug/mL streptomycin (Gibco). TRAMP-C2-sMICB and TRAMP-C2-MICB cell lines were generated with retroviral vector containing extracellular domain of MICB and full length of MICB respectively as previously described (17). PC3 cells were purchased from ATCC. The K562-CI9-mIL21 feeder cell line (CSTX002) was provided by Dr. Dean Lee under a material transfer agreement between Nationwide Children's Hospital and Northwestern University. All cell lines were authenticated by ATCC and were negative of mycoplasma contamination.

B10G5 and AB-K1 Antibodies

B10G5 is a murine monoclonal IgG1 antibody, recognizing soluble and membrane-bound MICA and MICB. Generation of B10G5 has been previously described (17). AB-K1 is a humanized B10G5 with the complementarity-determining region (CDR) grafting and human IgG1-Fc.

Animals

The generation and characterization of TRAMP/MICB and MICB/B6 transgenic mice have been previously described (17). NOD-*Prkdc*^{em26Cd52}*Il2rg*^{em26Cd22}/NjuCrl (NCG) mice were purchased

from Charles River. All mice used in this study were housed and bred under specific pathogen-free (SPF) conditions in the animal facility at Northwestern University in accordance with Institutional Animal Care and Use Committee (IACUC) approval. TRAMP/MICB were used at 24-32 weeks old. MICB/B6 and NCG mice are used at 12-16 weeks old.

Single cell RNA-sequencing of TILs from TRAMP/MICB prostate tumors

TRAMP/MICB mice were treated with the anti-MIC antibody B10G5 (200 ug) via intraperitoneal injections twice a week for 4 weeks. Prostate tumors from untreated and B10G5-treated TRAMP/MICB mice were treated with B10G5 (200 μg, intraperitoneally, twice weekly) for 4 weeks. Prostate tumors from untreated and B10G5-treated mice were collected, pooled, and processed into single-cell suspensions as previously described (19). Live CD45+ tumor-infiltrating leukocytes were sorted by flow cytometry after viability dye and CD45 staining, and scRNA-seq libraries were prepared using the Chromium Single Cell 3′ Kit v3 chemistry (10x Genomics). Sequencing was performed on an Illumina HiSeq 4000 using a 100-bp paired-end protocol.

scRNA-seq data were demultiplexed with Cell Ranger, aligned to the mouse mm10-2020-A reference genome, and analyzed using Seurat. After quality control, doublet removal, and filtering of cells with high feature counts, UMI counts, or mitochondrial gene expression, 17273 cells were retained. MALAT1 and mitochondrial genes were removed, and the top 2,000 highly variable genes were used for downstream analysis. Data were integrated with Harmony, followed by PCA, UMAP using the top 40 PCs, and clustering with FindNeighbors and FindClusters at a resolution of 0.8. NK cell clusters were identified by low *Cd3d/e* expression and enrichment of canonical NK markers, including *Klrb1c* and *Ncr1*. A total of 1,475 NK cells were subclustered at a resolution of 0.3. NK subcluster markers were identified using FindAllMarkers and ranked by

499 average log2FC. Trajectory analysis was performed using Slingshot and visualized using the SCP
500 package in R (v4.4.2).
501
502 **Flow cytometry**
503 For mouse tumoral NK cell analysis from TRAMP/MICB and subcutaneous syngeneic models,
504 tumors were mechanically dissociated into single-cell suspensions. Cells were stained with fixable
505 viability dye, Fc blocked, and surface stained to identify total NK cells (CD45+CD3-NK1.1+) and
506 NK cell subsets using antibodies against CXCR6, CD49a, NKG2A, LAG3, and/or KLRG1.
507 Intracellular staining for granzyme A, granzyme B, and perforin was performed using the
508 Cytofix/Cytoperm Fixation/Permeabilization Kit. Nuclear staining for EOMES, TCF1, and
509 KDM6B was performed using the FoxP3/Transcription Factor Staining Buffer Set. For
510 mitochondrial analyses, freshly processed cells were stained with MitoSOX, MitoTracker Deep
511 Red, and MitoTracker Green in RPMI with 10% FBS for 20 minutes at 37 °C. For human NK cell
512 profiling, antibodies against CD45, CD3, CD56, CD16, TCF1, EOMES, and KDM6B were used.
513 All antibodies used in this study are listed in Supplemental Table S3 with catalog number and
514 clone name provided.
515
516 **KDM6B Target Genes**
517 Putative KDM6B target genes and ChIP-seq peak-call data for mouse (mm10) and human (hg38)
518 were obtained from ChIP-Atlas (55), using a +/-1 kb distance from the TSS and an average
519 MACS2 score cutoff >20 (Q value < 0.01). H3K27me3 chromatin profiles in NK cells were
520 obtained from public GEO datasets (mouse NK cells, GSE222232; human NK cells, GSE209425)
521 (85, 86). Coverage plots were generated using the Gviz package in R.

Human pan-cancer NK cell scRNA-seq data analysis

The publicly available human tumor-infiltrating NK cell scRNA-seq dataset GSE212890 (56) was reanalyzed in R using Seurat v5.3.1. Cells labeled as "tumor" in the metadata were selected, and low-quality cells were removed using the following criteria: nFeature_RNA >200, nFeature_RNA <2500, and percent.mt <5. After normalization, feature selection, and scaling, the top 10 principal components were used for clustering at resolution 0.32 and UMAP dimensional reduction. Cluster markers were identified using FindAllMarkers.

Syngeneic mouse models of prostate cancer

Male MICB/B6 transgenic mice were used for syngeneic models of TRAMP-C2-sMICB or TRAMP-C2-MICB. Tumors were established by subcutaneous injection of TRAMP-C2-sMICB (1×10^6) or TRAMP-C2-MICB (2×10^6) onto the right flank. Tumor volume was calculated using the formula ($\text{width}^2 \times \text{length}$)/2. When tumor reached 75-100 mm^3, mice were randomized into treatment groups as specified in the figure legends. B10G5 (200 ug, BioXCell) was administered twice a week via intraperitoneal injections. For inhibition of KDM6B demethylase activities, GSK-J4 (10 mg/kg, MCE) was administered three times a week via intraperitoneal injections.

Stimulation of PBMCs

PBMCs were isolated from leukocyte reduction cones of healthy donors (purchased from Versiti Blood Center) and plated in anti-CD3 (OKT3, 1 ug/mL) coated 24-well plates with complete RPMI-1640 (Gibco) medium supplemented with 10% heat inactivated FBS (Hyclone), 100U U/mL penicillin, 100 ug/mL streptomycin (Gibco), and soluble anti-CD28 (CD28.2, 1 ug/mL).

The PBMCs were cultured with recombinant soluble MICA (Sino # 12302-H08H1), or MICB (Sino #10759-H08H), or pre-formed B10G5/sMIC complexes for 24 hours before flow cytometry analysis. B10G5/sMIC complexes were pre-formed by incubating recombinant MICA or MICB (100 ng/mL) with B10G5 at a B10G5-to-sMIC molar ratio of 0.3 in DPBS for 30 min at RT before addition to the culture.

Primary human NK cell expansion and culture

Human NK cells were expanded from healthy donor PBMCs using X-ray-irradiated K562-CI9-mIL21 feeder cells (generously shared by Dr. Dean Lee, Ohio State University Children's Hospital) for 10-14 days, as previously described (63). Cells were cultured in complete RPMI-1640 supplemented with 10% heat-inactivated FBS, penicillin/streptomycin, and 50 IU/mL human IL-2, with media refreshed every 2-3 days. NK cell purity was confirmed by flow cytometry to be >95% before use, with CD3 depletion performed when needed. For NCG xenograft studies, CD3 depletion was always performed on day 7. For B10G5-conditioned NK cells, B10G5 was maintained at 1 μg/mL throughout expansion. Before in vivo infusion, NK cells were washed and rested overnight in media containing 20 U/mL IL-2.

Immunofluorescence staining and imaging of KDM6B in NK cells

Primary human NK cells were stimulated with recombinant soluble MICA or MICB (Sino #12302-H08H1 or #10759-H08H) with or without anti-MIC antibody B10G5 for up to 5 days. Cells were fixed with 4% paraformaldehyde, attached to 0.01% poly-L-lysine-coated coverslips, permeabilized with 0.1% Triton X-100, blocked with 5% horse serum, and stained overnight at 4°C with anti-KDM6B rabbit polyclonal antibody (Abclonal A12763, 1:390), followed by

DyLight 650-conjugated anti-rabbit IgG (Abcam ab102294, 1:250) for 1 hour at room temperature. Cells were counterstained with Hoechst 33342 (Thermo Fisher), mounted with ProLong Diamond Antifade Mountant (Thermo Fisher), and imaged on a Leica DMi8 at 63x. Nuclear KDM6B fluorescence was quantified in ImageJ using Hoechst-based nuclear segmentation. KDM6B+ nuclei were defined by experiment-specific thresholds set by visual inspection, and the percentage of $KDM6B^+$ nuclei was calculated.

NK adoptive transfer therapy

Male NCG mice were implanted subcutaneously with PC3 human prostate cancer cells (5×10^6) into the right flank. When tumors reached 50 mm^3, mice were randomized into five groups: unconditioned NK cells, B10G5-conditioned NK cells, unconditioned NK cells plus AB-K1, B10G5-conditioned NK cells plus AB-K1, or no treatment. NK cells (1×10^7) were injected intravenously once every 7-12 days for three total doses. AB-K1 (100 μg) was administered intraperitoneally twice weekly, and IL-2 (10,000 IU per mouse) was administered intraperitoneally three times weekly to support NK cell survival. Mice were euthanized 5 days after the final NK cell injection.

CUT&RUN followed by quantitative PCR (CUT&RUN-qPCR)

Primary human NK cells were stimulated with recombinant sMIC, preformed B10G5/sMIC complex, or vehicle control. CUT&RUN was performed using the CUT&RUN Assay Kit (Cell Signaling Technology #86652) with 250,000 live cells per reaction and anti-H3K27me3 antibody (#9733, 1:50) or rabbit IgG control (#66362). After pAG-MNase-mediated cleavage, yeast spike-in DNA (#36598) was added for normalization. Input DNA was prepared by sonication, and

enriched and input DNA were purified using Cell Signaling Technology buffers and columns (#14209). qPCR was performed with SsoAdvanced Universal SYBR Green Supermix and primers listed in Supplemental Table S4. Enrichment was calculated as % input, normalized to yeast spike-in DNA, and expressed as fold enrichment relative to vehicle control.

Statistical analysis

Unless stated otherwise, statistical significance of differences between groups was determined by two-tailed, unpaired Welch's t-tests, two-way ANOVA, one-way ANOVA with Tukey's multiple comparison tests, or Friedman tests with Dunn's multiple comparisons tests as specified in the figure legends using GraphPad Prism (v10.5.0). $P < 0.05$ was considered statistically significant. The error bars show Standard Error of the Mean (SEM).

Study approval

All animal studies were approved by the Northwestern University Institutional Animal Care and Use Committee (IACUC). Human PBMCs from healthy donors were isolated from de-identified leukocyte reduction cones purchased from Versiti Blood Center, obtained under Versiti's approved donor consent and anonymization procedures. This study qualified as exempt human subjects research under Northwestern Institutional Review Board (IRB) policies.

Data availability

The scRNA-seq data generated in this study have been uploaded to the Gene Expression Omnibus (GSE309465). No original code was generated. Analysis code is available at https://github.com/Wu-Lab-NU/B10G5-reshapes-tumor-immune-contexture. Graph datapoints

are provided in the Supporting Data Values file. Further information is available from the corresponding author upon reasonable request.

Manuscript Information

Author contributions

JW and SL were responsible for conception and design of the study. SL, PD, TAS, KG and AG conducted experiments and acquired data. SL, RJB, GPY and JW analyzed and interpreted data. SL, BZ, DF, CH, DV, MK, SMP, QM, QC, WC, JW wrote and reviewed the manuscript. JW supervised the study. Authors were orderly according to contributions to this study.

AI disclosure

The authors declare that no AI tools were used in the original research for or writing of this article.

Conflict of Interest

J. Wu is the inventor of the B10G5 antibody and has international patent applications. All other authors declare no conflict of interest.

Funding support

This work is the result of NIH funding, in whole or in part, and is subject to the NIH Public Access Policy. Through acceptance of this federal funding, the NIH has been given a right to make the work publicly available in PubMed Central. This work was supported by NIH/NCI grants R01CA284640 and R01CA290719 and USAMRDC Award W81XWH-21-1-0574 to JW and Prostate SPORE P50CA180995.

Acknowledgements

We thank the Lurie Comprehensive Cancer Center Flow Cytometry Core Facility, supported in part by NCI Cancer Center Support Grant P30 CA060553, and the University of Chicago Functional Genomics Core (RRID:SCR_019196) for sequencing services. Some figures were generated with BioRender.com (Figure 1A, Supplemental Figures 4B-C and 12C, and Graphical Abstract). We also thank Dr. Ju Wu, Dr. Sheng-Xian Jia, and Annie Yoo Kyung Lee for assistance with tissue collection.

Address for correspondence

Jennifer D. Wu, PhD and Professor, 303 E. Superior St., Lurie Research Building 6-117

Chicago, IL60611, jennifer.wu@northwestern.edu. Phone (312) 503 1521.

References

1. Liu E, Marin D, Banerjee P, Macapinlac HA, Thompson P, Basar R, et al. Use of CAR-Transduced Natural Killer Cells in CD19-Positive Lymphoid Tumors. *N Engl J Med.* 2020;382(6):545–53.
2. Nieto Y, Banerjee P, Kaur I, Basar R, Li Y, Daher M, et al. Allogeneic NK cells with a bispecific innate cell engager in refractory relapsed lymphoma: a phase 1 trial. *Nat Med.* 2025;31(6):1987–93.
3. Wang W, Liu Y, He Z, Li L, Liu S, Jiang M, et al. Breakthrough of solid tumor treatment: CAR-NK immunotherapy. *Cell Death Discov.* 2024;10(1):40.
4. Dhar P, and Wu JD. NKG2D and its ligands in cancer. *Curr Opin Immunol.* 2018;51:55–61.
5. Blery M, Mrabet-Kraiem M, Morel A, Lhospice F, Bregeon D, Bonnafous C, et al. Targeting MICA/B with cytotoxic therapeutic antibodies leads to tumor control [version 2; peer review: 2 approved]. *Open Res Eur.* 2021;1:107.
6. Bauer S, Groh V, Wu J, Steinle A, Phillips JH, Lanier LL, et al. Activation of NK cells and T cells by NKG2D, a receptor for stress-inducible MICA. *Science.* 1999;285(5428):727–9.
7. Gasser S, and Raulet D. The DNA damage response, immunity and cancer. *Semin Cancer Biol.* 2006;16(5):344–7.
8. Nausch N, and Cerwenka A. NKG2D ligands in tumor immunity. *Oncogene.* 2008;27(45):5944–58.

9. Groh V, Bahram S, Bauer S, Herman A, Beauchamp M, and Spies T. Cell stress-regulated human major histocompatibility complex class I gene expressed in gastrointestinal epithelium. *Proc Natl Acad Sci U S A.* 1996;93(22):12445–50.

10. Wang X, Lundgren AD, Singh P, Goodlett DR, Plymate SR, and Wu JD. An six-amino acid motif in the alpha3 domain of MICA is the cancer therapeutic target to inhibit shedding. *Biochem Biophys Res Commun.* 2009;387(3):476–81.

11. Ferrari de Andrade L, Tay RE, Pan D, Luoma AM, Ito Y, Badrinath S, et al. Antibody-mediated inhibition of MICA and MICB shedding promotes NK cell-driven tumor immunity. *Science.* 2018;359(6383):1537–42.

12. Groh V, Wu J, Yee C, and Spies T. Tumour-derived soluble MIC ligands impair expression of NKG2D and T-cell activation. *Nature.* 2002;419(6908):734–8.

13. Salih HR, Holdenrieder S, and Steinle A. Soluble NKG2D ligands: prevalence, release, and functional impact. *Front Biosci.* 2008;13:3448–56.

14. Baragano Raneros A, Suarez-Alvarez B, and Lopez-Larrea C. Secretory pathways generating immunosuppressive NKG2D ligands: New targets for therapeutic intervention. *Oncoimmunology.* 2014;3:e28497.

15. Holdenrieder S, Stieber P, Peterfi A, Nagel D, Steinle A, and Salih HR. Soluble MICA in malignant diseases. *Int J Cancer.* 2006;118(3):684–7.

16. Holdenrieder S, Stieber P, Peterfi A, Nagel D, Steinle A, and Salih HR. Soluble MICB in malignant diseases: analysis of diagnostic significance and correlation with soluble MICA. *Cancer Immunol Immunother.* 2006;55(12):1584–9.

17. Liu G, Lu S, Wang X, Page ST, Higano CS, Plymate SR, et al. Perturbation of NK cell peripheral homeostasis accelerates prostate carcinoma metastasis. *J Clin Invest.* 2013;123(10):4410–22.

18. Wu JD, Higgins LM, Steinle A, Cosman D, Haugk K, and Plymate SR. Prevalent expression of the immunostimulatory MHC class I chain-related molecule is counteracted by shedding in prostate cancer. *J Clin Invest.* 2004;114(4):560–8.

19. Jinushi M, Hodi FS, and Dranoff G. Therapy-induced antibodies to MHC class I chain-related protein A antagonize immune suppression and stimulate antitumor cytotoxicity. *Proceedings of the National Academy of Sciences of the United States of America.* 2006;103(24):9190–5.

20. Jinushi M, Vanneman M, Munshi NC, Tai YT, Prabhala RH, Ritz J, et al. MHC class I chain-related protein A antibodies and shedding are associated with the progression of multiple myeloma. *Proceedings of the National Academy of Sciences of the United States of America.* 2008;105(4):1285–90.

21. Wu JD, Atteridge CL, Wang X, Seya T, and Plymate SR. Obstructing shedding of the immunostimulatory MHC class I chain-related gene B prevents tumor formation. *Clin Cancer Res.* 2009;15(2):632–40.

22. Hanaoka N, Jabri B, Dai Z, Ciszewski C, Stevens AM, Yee C, et al. NKG2D initiates caspase-mediated CD3zeta degradation and lymphocyte receptor impairments associated with human cancer and autoimmune disease. *J Immunol.* 2010;185(10):5732–42.

23. Coudert JD, Scarpellino L, Gros F, Vivier E, and Held W. Sustained NKG2D engagement induces cross-tolerance of multiple distinct NK cell activation pathways. *Blood.* 2008;111(7):3571–8.

24. Coudert JD, Zimmer J, Tomasello E, Cebecauer M, Colonna M, Vivier E, et al. Altered NKG2D function in NK cells induced by chronic exposure to NKG2D ligand-expressing tumor cells. *Blood.* 2005;106(5):1711–7.

25. Dhar P, Basher F, Ji Z, Huang L, Qin S, Wainwright DA, et al. Tumor-derived NKG2D ligand sMIC reprograms NK cells to an inflammatory phenotype through CBM signalosome activation. *Commun Biol.* 2021;4(1):905.

26. Lu S, Zhang J, Liu D, Li G, Staveley-O'Carroll KF, Li Z, et al. Nonblocking Monoclonal Antibody Targeting Soluble MIC Revamps Endogenous Innate and Adaptive Antitumor Responses and Eliminates Primary and Metastatic Tumors. *Clin Cancer Res.* 2015;21(21):4819–30.

27. Bahram S, and Spies T. The MIC gene family. *Res Immunol.* 1996;147(5):328–33.

28. Kasahara M, and Yoshida S. Immunogenetics of the NKG2D ligand gene family. *Immunogenetics.* 2012;64(12):855–67.

29. Basher F, Dhar P, Wang X, Wainwright DA, Zhang B, Sosman J, et al. Antibody targeting tumor-derived soluble NKG2D ligand sMIC reprograms NK cell homeostatic survival and function and enhances melanoma response to PDL1 blockade therapy. *J Hematol Oncol.* 2020;13(1):74.

30. Basher F, Jeng EK, Wong H, and Wu J. Cooperative therapeutic anti-tumor effect of IL-15 agonist ALT-803 and co-targeting soluble NKG2D ligand sMIC. *Oncotarget.* 2016;7(1):814–30.

31. Wu T, Ji Y, Moseman EA, Xu HC, Manglani M, Kirby M, et al. The TCF1-Bcl6 axis counteracts type I interferon to repress exhaustion and maintain T cell stemness. *Sci Immunol.* 2016;1(6).

746 32. Li G, Yang Q, Zhu Y, Wang HR, Chen X, Zhang X, et al. T-Bet and Eomes Regulate the
747 Balance between the Effector/Central Memory T Cells versus Memory Stem Like T
748 Cells. *PLoS One.* 2013;8(6):e67401.
749 33. Gautam S, Fioravanti J, Zhu W, Le Gall JB, Brohawn P, Lacey NE, et al. The
750 transcription factor c-Myb regulates CD8(+) T cell stemness and antitumor immunity.
751 *Nat Immunol.* 2019;20(3):337–49.
752 34. Lin S, Niu H, Zhang Y, Gai K, Brown R, Brown A, et al. SATB1 is a key regulator of
753 quiescence in stem-like CD8(+) T cells. *Nat Immunol.* 2025.
754 35. Liu J, Wang Z, Hao S, Wang F, Yao Y, Zhang Y, et al. Tcf1 Sustains the Expression of
755 Multiple Regulators in Promoting Early Natural Killer Cell Development. *Front*
756 *Immunol.* 2021;12:791220.
757 36. Jeevan-Raj B, Gehrig J, Charmoy M, Chennupati V, Grandclement C, Angelino P, et al.
758 The Transcription Factor Tcf1 Contributes to Normal NK Cell Development and Function
759 by Limiting the Expression of Granzymes. *Cell Rep.* 2017;20(3):613–26.
760 37. Voskoboinik I, Smyth MJ, and Trapani JA. Perforin-mediated target-cell death and
761 immune homeostasis. *Nat Rev Immunol.* 2006;6(12):940–52.
762 38. Voskoboinik I, Whisstock JC, and Trapani JA. Perforin and granzymes: function,
763 dysfunction and human pathology. *Nat Rev Immunol.* 2015;15(6):388–400.
764 39. Berrien-Elliott MM, Cashen AF, Cubitt CC, Neal CC, Wong P, Wagner JA, et al.
765 Multidimensional Analyses of Donor Memory-Like NK Cells Reveal New Associations
766 with Response after Adoptive Immunotherapy for Leukemia. *Cancer Discov.*
767 2020;10(12):1854–71.

40. Berrien-Elliott MM, Foltz JA, Russler-Germain DA, Neal CC, Tran J, Gang M, et al. Hematopoietic cell transplantation donor-derived memory-like NK cells functionally persist after transfer into patients with leukemia. *Sci Transl Med.* 2022;14(633):eabm1375.

41. Lieberman J. Granzyme A activates another way to die. *Immunol Rev.* 2010;235(1):93–104.

42. Jia H, Yang H, Xiong H, and Luo KQ. NK cell exhaustion in the tumor microenvironment. *Front Immunol.* 2023;14:1303605.

43. Huntington ND, Tabarias H, Fairfax K, Brady J, Hayakawa Y, Degli-Esposti MA, et al. NK cell maturation and peripheral homeostasis is associated with KLRG1 up-regulation. *J Immunol.* 2007;178(8):4764–70.

44. Poznanski SM, Singh K, Ritchie TM, Aguiar JA, Fan IY, Portillo AL, et al. Metabolic flexibility determines human NK cell functional fate in the tumor microenvironment. *Cell Metab.* 2021;33(6):1205–20 e5.

45. Zheng X, Qian Y, Fu B, Jiao D, Jiang Y, Chen P, et al. Mitochondrial fragmentation limits NK cell-based tumor immunosurveillance. *Nat Immunol.* 2019;20(12):1656–67.

46. Solaini G, Baracca A, Lenaz G, and Sgarbi G. Hypoxia and mitochondrial oxidative metabolism. *Biochim Biophys Acta.* 2010;1797(6-7):1171–7.

47. Gorrini C, Harris IS, and Mak TW. Modulation of oxidative stress as an anticancer strategy. *Nat Rev Drug Discov.* 2013;12(12):931–47.

48. Redza-Dutordoir M, and Averill-Bates DA. Activation of apoptosis signalling pathways by reactive oxygen species. *Biochim Biophys Acta.* 2016;1863(12):2977–92.

49. Srinivas US, Tan BWQ, Vellayappan BA, and Jeyasekharan AD. ROS and the DNA damage response in cancer. *Redox Biol.* 2019;25:101084.

50. Lu L, Yang C, Zhou X, Wu L, Hong X, Li W, et al. STING signaling promotes NK cell antitumor immunity and maintains a reservoir of TCF-1(+) NK cells. *Cell Rep.* 2023;42(9):113108.

51. Kang TG, Lan X, Mi T, Chen H, Alli S, Lim SE, et al. Epigenetic regulators of clonal hematopoiesis control CD8 T cell stemness during immunotherapy. *Science.* 2024;386(6718):eadl4492.

52. Pace L, Goudot C, Zueva E, Gueguen P, Burgdorf N, Waterfall JJ, et al. The epigenetic control of stemness in CD8(+) T cell fate commitment. *Science.* 2018;359(6372):177–86.

53. Salminen A, Kaarniranta K, Hiltunen M, and Kauppinen A. Histone demethylase Jumonji D3 (JMJD3/KDM6B) at the nexus of epigenetic regulation of inflammation and the aging process. *J Mol Med (Berl).* 2014;92(10):1035–43.

54. Mallaney C, Ostrander EL, Celik H, Kramer AC, Martens A, Kothari A, et al. Kdm6b regulates context-dependent hematopoietic stem cell self-renewal and leukemogenesis. *Leukemia.* 2019;33(10):2506–21.

55. Zou Z, Ohta T, Miura F, and Oki S. ChIP-Atlas 2021 update: a data-mining suite for exploring epigenomic landscapes by fully integrating ChIP-seq, ATAC-seq and Bisulfite-seq data. *Nucleic Acids Res.* 2022;50(W1):W175–W82.

56. Tang F, Li J, Qi L, Liu D, Bo Y, Qin S, et al. A pan-cancer single-cell panorama of human natural killer cells. *Cell.* 2023;186(19):4235–51 e20.

57. Miller SA, Mohn SE, and Weinmann AS. Jmjd3 and UTX play a demethylase-independent role in chromatin remodeling to regulate T-box family member-dependent gene expression. *Molecular cell.* 2010;40(4):594–605.

58. Vicioso-Mantis M, Fueyo R, Navarro C, Cruz-Molina S, van Ijcken WFJ, Rebollo E, et al. JMJD3 intrinsically disordered region links the 3D-genome structure to TGFbeta-dependent transcription activation. *Nat Commun.* 2022;13(1):3263.

59. Wong P, Foltz JA, Chang L, Neal CC, Yao T, Cubitt CC, et al. T-BET and EOMES sustain mature human NK cell identity and antitumor function. *J Clin Invest.* 2023;133(13).

60. Gill S, Vasey AE, De Souza A, Baker J, Smith AT, Kohrt HE, et al. Rapid development of exhaustion and down-regulation of eomesodermin limit the antitumor activity of adoptively transferred murine natural killer cells. *Blood.* 2012;119(24):5758–68.

61. Kamikawa YF, and Donohoe ME. The localization of histone H3K27me3 demethylase Jmjd3 is dynamically regulated. *Epigenetics.* 2014;9(6):834–41.

62. Yang SG, Li CP, Wang XW, Huang T, Qian C, Li Q, et al. Roles of Kdm6a and Kdm6b in Regulation of Mammalian Neural Regeneration. *Adv Sci (Weinh).* 2025;12(16):e2405537.

63. Denman CJ, Senyukov VV, Somanchi SS, Phatarpekar PV, Kopp LM, Johnson JL, et al. Membrane-bound IL-21 promotes sustained ex vivo proliferation of human natural killer cells. *PLoS One.* 2012;7(1):e30264.

64. Ciurea SO, Schafer JR, Bassett R, Denman CJ, Cao K, Willis D, et al. Phase 1 clinical trial using mbIL21 ex vivo-expanded donor-derived NK cells after haploidentical transplantation. *Blood.* 2017;130(16):1857–68.

65. Geller MA, Cooley S, Judson PL, Ghebre R, Carson LF, Argenta PA, et al. A phase II study of allogeneic natural killer cell therapy to treat patients with recurrent ovarian and breast cancer. *Cytotherapy.* 2011;13(1):98–107.

66. Lozzio CB, and Lozzio BB. Human chronic myelogenous leukemia cell-line with positive Philadelphia chromosome. *Blood.* 1975;45(3):321–34.

67. Whalen KA, Henry CC, Mehta NK, Rakhra K, Yalcin S, Meetze K, et al. CLN-619, a MICA/B monoclonal antibody that promotes innate immune cell-mediated antitumor activity. *J Immunother Cancer.* 2025;13(4).

68. Kowash RR, Sabnani M, Gray LT, Deng Q, Saleh NUA, Girard L, et al. Novel and potent MICA/B antibody is therapeutically effective in KRAS LKB1 mutant lung cancer models. *J Immunother Cancer.* 2025;13(1).

69. Du C, Bevers J, 3rd, Cook R, Lombana TN, Rajasekaran K, Matsumoto M, et al. MICA immune complex formed with alpha 3 domain-specific antibody activates human NK cells in a Fc-dependent manner. *J Immunother Cancer.* 2019;7(1):207.

70. Wensveen FM, Jelencic V, and Polic B. NKG2D: A Master Regulator of Immune Cell Responsiveness. *Front Immunol.* 2018;9:441.

71. Klose CSN, Flach M, Mohle L, Rogell L, Hoyler T, Ebert K, et al. Differentiation of type 1 ILCs from a common progenitor to all helper-like innate lymphoid cell lineages. *Cell.* 2014;157(2):340–56.

72. Romee R, Schneider SE, Leong JW, Chase JM, Keppel CR, Sullivan RP, et al. Cytokine activation induces human memory-like NK cells. *Blood.* 2012;120(24):4751–60.

73. Romee R, Rosario M, Berrien-Elliott MM, Wagner JA, Jewell BA, Schappe T, et al. Cytokine-induced memory-like natural killer cells exhibit enhanced responses against myeloid leukemia. *Sci Transl Med.* 2016;8(357):357ra123.

74. Foltz JA, Tran J, Wong P, Fan C, Schmidt E, Fisk B, et al. Cytokines drive the formation of memory-like NK cell subsets via epigenetic rewiring and transcriptional regulation. *Sci Immunol.* 2024;9(96):eadk4893.

75. Estaras C, Fueyo R, Akizu N, Beltran S, and Martinez-Balbas MA. RNA polymerase II progression through H3K27me3-enriched gene bodies requires JMJD3 histone demethylase. *Mol Biol Cell.* 2013;24(3):351–60.

76. Chen S, Ma J, Wu F, Xiong LJ, Ma H, Xu W, et al. The histone H3 Lys 27 demethylase JMJD3 regulates gene expression by impacting transcriptional elongation. *Genes Dev.* 2012;26(12):1364–75.

77. Chakraborty AA, Laukka T, Myllykoski M, Ringel AE, Booker MA, Tolstorukov MY, et al. Histone demethylase KDM6A directly senses oxygen to control chromatin and cell fate. *Science.* 2019;363(6432):1217–22.

78. Xu T, Schutte A, Jimenez L, Goncalves ANA, Keller A, Pipkin ME, et al. Kdm6b Regulates the Generation of Effector CD8(+) T Cells by Inducing Chromatin Accessibility in Effector-Associated Genes. *J Immunol.* 2021;206(9):2170–83.

79. Li J, Hardy K, Olshansky M, Barugahare A, Gearing LJ, Prier JE, et al. KDM6B-dependent chromatin remodeling underpins effective virus-specific CD8(+) T cell differentiation. *Cell Rep.* 2021;34(11):108839.

80. Ford BR, Vignali PDA, Rittenhouse NL, Scharping NE, Peralta R, Lontos K, et al. Tumor microenvironmental signals reshape chromatin landscapes to limit the functional potential of exhausted T cells. *Sci Immunol.* 2022;7(74):eabj9123.

81. Cribbs A, Hookway ES, Wells G, Lindow M, Obad S, Oerum H, et al. Inhibition of histone H3K27 demethylases selectively modulates inflammatory phenotypes of natural killer cells. *The Journal of biological chemistry.* 2018;293(7):2422–37.

82. Scharping NE, Menk AV, Moreci RS, Whetstone RD, Dadey RE, Watkins SC, et al. The Tumor Microenvironment Represses T Cell Mitochondrial Biogenesis to Drive Intratumoral T Cell Metabolic Insufficiency and Dysfunction. *Immunity.* 2016;45(2):374–88.

83. Kim D, Kim G, Yu R, Lee J, Kim S, Gleason MR, et al. Inhibitory co-receptor Lag3 supports Foxp3(+) regulatory T cell function by restraining Myc-dependent metabolic programming. *Immunity.* 2024;57(11):2634–50 e5.

84. Zhang X, Chen H, Han J, Wang Z, Guo Y, Zhou Z, et al. ATM-AMPKalpha mediated LAG-3 expression suppresses T cell function in prostate cancer. *Cell Immunol.* 2023;393-394:104773.

85. Sudholz H, Schuster IS, Foroutan M, Sng X, Andoniou CE, Doan A, et al. DOT1L maintains NK cell phenotype and function for optimal tumor control. *Cell Rep.* 2024;43(6):114333.

86. Consortium EP. An integrated encyclopedia of DNA elements in the human genome. *Nature.* 2012;489(7414):57–74.

898 **Graphical Abstract**

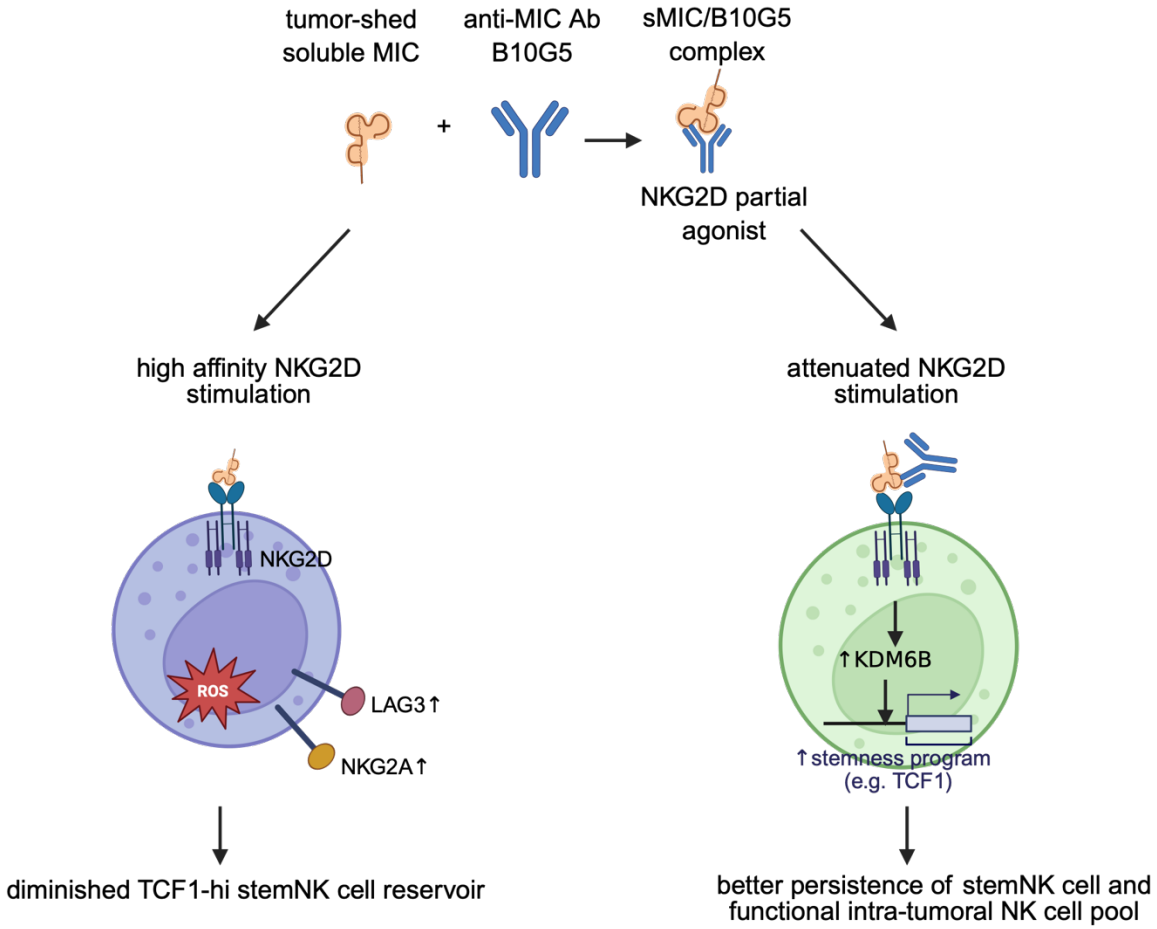

899
900

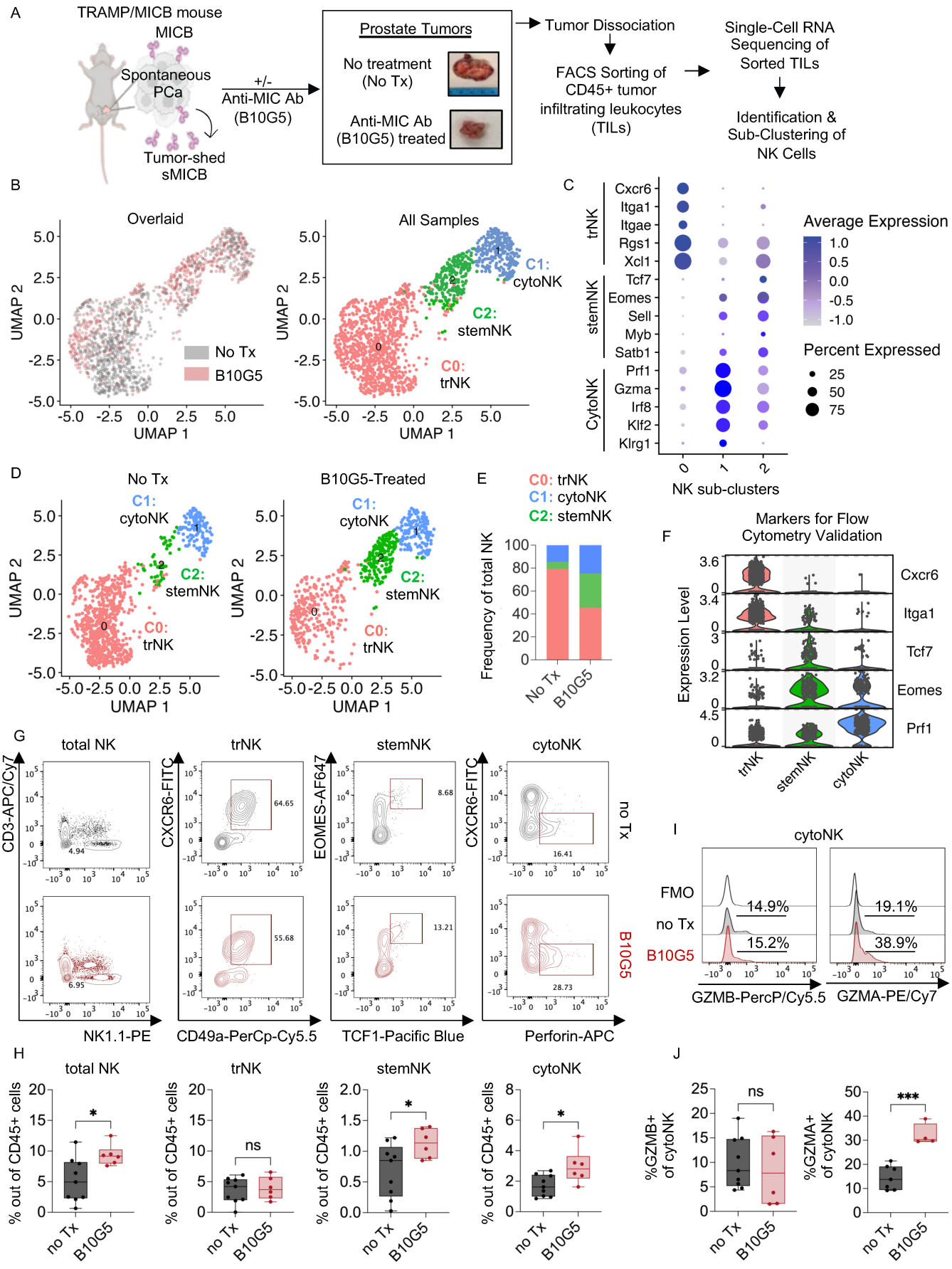
A
TRAMP/MICB mouse
MICB
Spontaneous PCa
Tumor-shed sMICB
+/- Anti-MIC Ab (B10G5)
Prostate Tumors
No treatment (No Tx)
Anti-MIC Ab (B10G5) treated
Tumor Dissociation
FACS Sorting of CD45+ tumor infiltrating leukocytes (TILs)
Single-Cell RNA Sequencing of Sorted TILs
Identification & Sub-Clustering of NK Cells
B
Overlaid
All Samples
UMAP 1
UMAP 2
No Tx
B10G5
C0: trNK
C1: cytoNK
C2: stemNK
C
trNK
stemNK
CytoNK
Cxcr6
Itga1
Itgae
Rgs1
Xcl1
Tcf7
Eomes
Sell
Myb
Satb1
Prf1
Gzma
Irf8
Klf2
Klrg1
Average Expression
Percent Expressed
NK sub-clusters
D
No Tx
B10G5-Treated
E
Frequency of total NK
F
Markers for Flow Cytometry Validation
Expression Level
G
total NK
trNK
stemNK
cytoNK
CD3-APC/Cy7
NK1.1-PE
CXCR6-FITC
CD49a-PerCp-Cy5.5
EOMES-AF647
TCF1-Pacific Blue
Perforin-APC
no Tx
B10G5
I
FMO
14.9%
15.2%
19.1%
38.9%
GZMB-PercP/Cy5.5
GZMA-PE/Cy7
H
% out of CD45+ cells
ns
J
%GZMB+ of cytoNK
%GZMA+ of cytoNK
***

901

Figure 1. Attenuating NKG2D stimulation enriches intratumoral EOMES^{hi}TCF1^{hi} stemNK cells and preserves NK cell functional diversity.

(A) scRNA-seq was performed on live CD45+ cells FACS-sorted from prostate tumors of untreated and B10G5-treated TRAMP/MICB mice. (B) UMAP of NK-cell subclusters after immune-cell annotation and NK-cell re-clustering. (C) Dot plot of representative marker genes for each NK-cell subcluster, identified by Seurat FindAllMarkers and ranked by average log2FC; top markers are listed in Supplemental Table S1. (D) UMAPs showing NK-cell subclusters by sample. (E) Frequencies of NK-cell subclusters among total NK cells in untreated and B10G5-treated samples. (F) Violin plots of key markers used for flow cytometry validation. (G) Representative flow cytometry contour plots of total tumoral NK cells (CD3$^-$NK1.1$^+$) and trNK (CXCR6$^+$CD49a$^+$), stemNK (EOMES^{hi}TCF1^{hi}), and cytoNK (CXCR6$^-$Perforin^{hi}) subsets; full gating is shown in Supplemental Figure 3. (H) Percentage of total NK cells, trNK cells, stemNK cells and cytoNK cells out of CD45$^+$ intra-tumoral immune cells (n=9 mice (no Tx) and 6 mice (B10G5)). (I-J) Frequencies of GZMB$^+$ cytoNK cells (untreated n=9; B10G5 n=6) and GZMA$^+$ cytoNK cells (untreated n=7; B10G5 n=4). Flow cytometry data were analyzed by Welch's t-tests (H, J). Box plots show all data points; boxes and lines indicate minimum, 25th percentile, median, 75th percentile, and maximum values. *$p < 0.05$, **$p < 0.01$, ***$p < 0.001$.

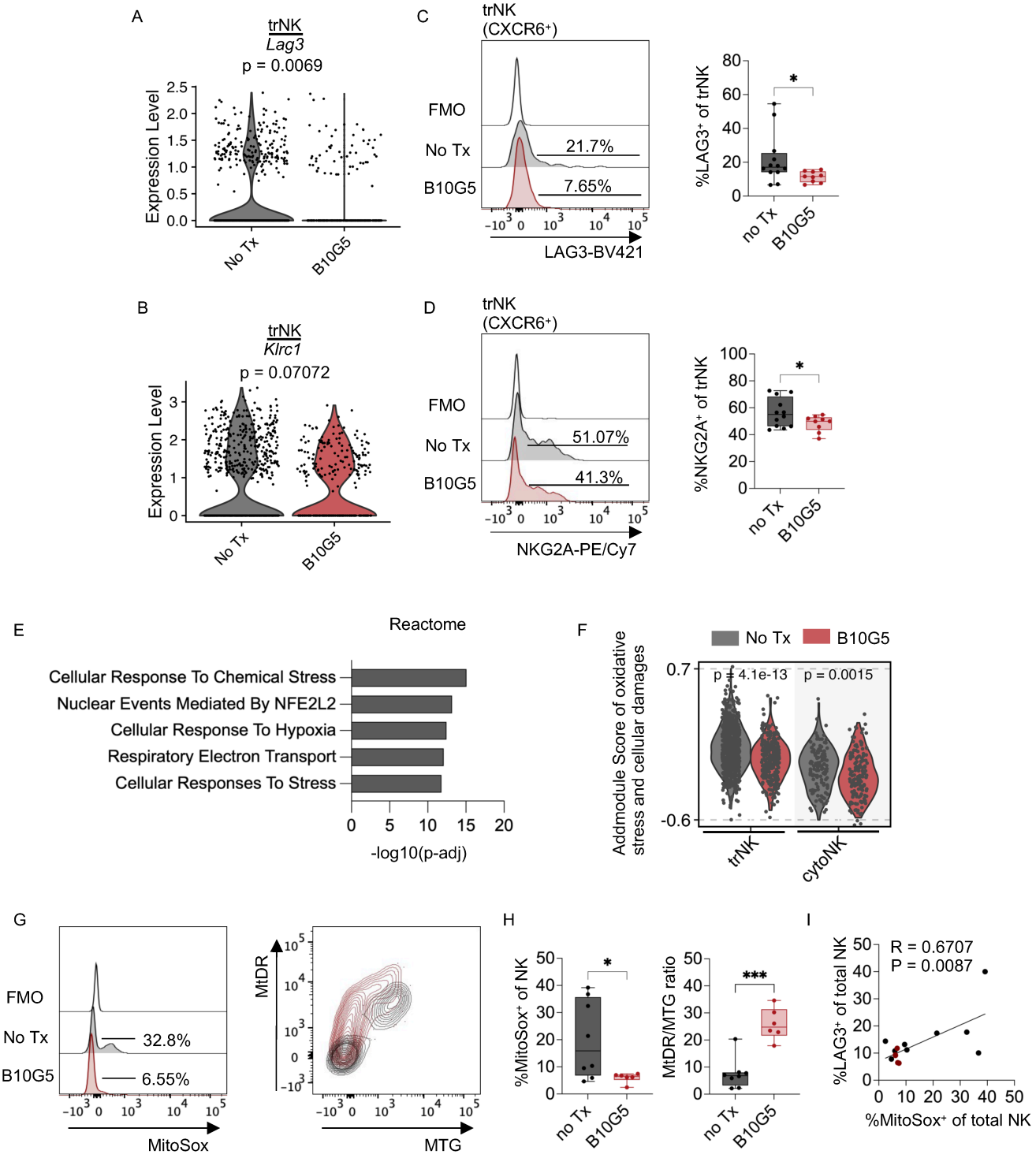
A
trNK
Lag3
p = 0.0069
Expression Level
No Tx
B10G5
B
trNK
Klrc1
p = 0.07072
Expression Level
No Tx
B10G5
C
trNK
(CXCR6+)
FMO
No Tx
B10G5
21.7%
7.65%
LAG3-BV421
%LAG3+ of trNK
no Tx
B10G5
D
trNK
(CXCR6+)
FMO
No Tx
B10G5
51.07%
41.3%
NKG2A-PE/Cy7
%NKG2A+ of trNK
no Tx
B10G5
E
Reactome
Cellular Response To Chemical Stress
Nuclear Events Mediated By NFE2L2
Cellular Response To Hypoxia
Respiratory Electron Transport
Cellular Responses To Stress
-log10(p-adj)
F
No Tx
B10G5
Addmodule Score of oxidative stress and cellular damages
p = 4.1e-13
p = 0.0015
trNK
cytoNK
G
FMO
No Tx
B10G5
32.8%
6.55%
MitoSox
MtDR
MTG
H
%MitoSox+ of NK
no Tx
B10G5
MtDR/MTG ratio
no Tx
B10G5
I
R = 0.6707
P = 0.0087
%LAG3+ of total NK
%MitoSox+ of total NK

Figure 2. Attenuating NKG2D stimulation mitigates sMIC-induced NK cell exhaustion and oxidative stress.

(A-B) Violin plots showing *Lag3* and *Klrc1* (encoding NKG2A) expression at the transcript level in trNK cells from the scRNA-seq dataset. (C-D) LAG3 and NKG2A expression at the protein level on trNK cells from untreated (n=12) or B10G5-treated (n=9) TRAMP/MICB tumors. The boxplots show percentage of marker positive cells out of trNK. (E) Select Reactome pathways upregulated in untreated NK cells compared to B10G5-treated ones using EnrichR. (F) Oxidative stress and cellular damage module scores calculated with Seurat AddModuleScore; individual genes are shown in Supplemental Figure 6A. (G-H) Flow cytometric analysis of MitoSOX and MitoTracker staining in NK cells from untreated (n=8) and B10G5-treated (n=6) TRAMP/MICB tumors. (I) Pearson correlation of %LAG3^{+} and %MitoSox^{+} of total tumoral NK cells. Statistical analyses were performed using Wilcoxon tests for scRNA-seq data (A-B, F) and Welch's t-tests for flow cytometry data (C-D, H). Box plots (C-D, H) showed all datapoints; boxes and lines indicate minimum, 25th percentile, median, 75th percentile, and maximum values. *$p < 0.05$, **$p < 0.01$, ***$p < 0.001$.

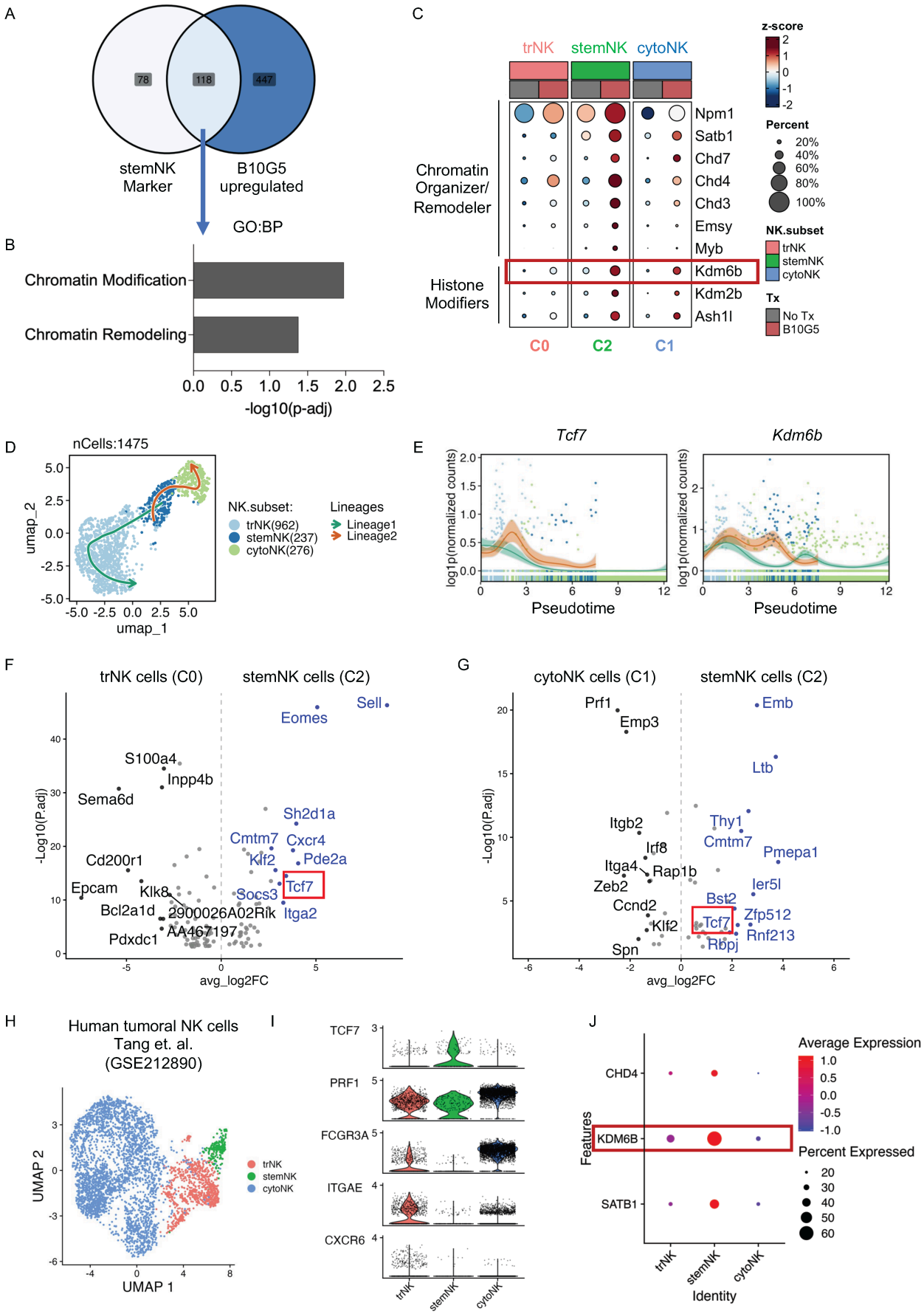
A
78
118
447
stemNK Marker
B10G5 upregulated
GO:BP
B
Chromatin Modification
Chromatin Remodeling
0.0 0.5 1.0 1.5 2.0 2.5
-log10(p-adj)
C
trNK stemNK cytoNK
Chromatin Organizer/ Remodeler
Histone Modifiers
Npm1
Satb1
Chd7
Chd4
Chd3
Emsy
Myb
Kdm6b
Kdm2b
Ash1l
C0 C2 C1
z-score
Percent
20%
40%
60%
80%
100%
NK.subset
trNK
stemNK
cytoNK
Tx
No Tx
B10G5
D
nCells:1475
umap_2
umap_1
NK.subset:
trNK(962)
stemNK(237)
cytoNK(276)
Lineages
Lineage1
Lineage2
E
Tcf7
Kdm6b
log1p(normalized counts)
Pseudotime
F
trNK cells (C0)
stemNK cells (C2)
-Log10(P.adj)
avg_log2FC
Sell
Eomes
S100a4
Inpp4b
Sema6d
Sh2d1a
Cmtm7
Cxcr4
Klf2
Pde2a
Cd200r1
Epcam
Klk8
Tcf7
Socs3
Itga2
Bcl2a1d
2900026A02Rik
AA467197
Pdxdc1
G
cytoNK cells (C1)
stemNK cells (C2)
Prf1
Emp3
Emb
Ltb
Thy1
Itgb2
Cmtm7
Irf8
Pmepa1
Itga4
Rap1b
Zeb2
Ier5l
Bst2
Ccnd2
Zfp512
Klf2
Tcf7
Rnf213
Rbpj
Spn
H
Human tumoral NK cells
Tang et. al.
(GSE212890)
UMAP 2
UMAP 1
trNK
stemNK
cytoNK
I
TCF7
PRF1
FCGR3A
ITGAE
CXCR6
trNK
stemNK
cytoNK
J
Average Expression
Percent Expressed
CHD4
KDM6B
SATB1
Features
Identity
trNK
stemNK
cytoNK

937

Figure 3. KDM6B is identified as a candidate regulator of NK cell stemness.

(A) Genes overlapping between stemNK cell markers and B10G5-upregulated DEGs were identified and analyzed for pathway enrichment with EnrichR. (B) Select enriched Gene Ontology Biological Process (GO:BP) pathways for the overlapping genes. (C) Dot plot showing expression of genes in the chromatin remodeling and modification pathways. (D) Trajectory analysis of the mouse tumoral NK cell subsets using slingshot revealed two potential lineages. (E) *Tcf7* and *Kdm6b* expression along pseudotime of the trajectories. (F) KDM6B targets (obtained using CHIP-Atlas) in DEGs between stemNK (C2) and trNK (C0) cells. (G) KDM6B targets in DEGs between stemNK (C2) and cytoNK (C1) cells. (H) A public human pan-cancer scRNA-seq dataset for tumoral NK cells (GSE212890, Tang et. al) was re-analyzed, revealing trNK, cytoNK and stemNK cell subsets infiltrating human tumors. (I) Key markers defining each human tumoral NK cell subset. (J) Dot plot showing expression of select epigenetic modifiers identified in (B-C) in human tumoral NK cell subsets.

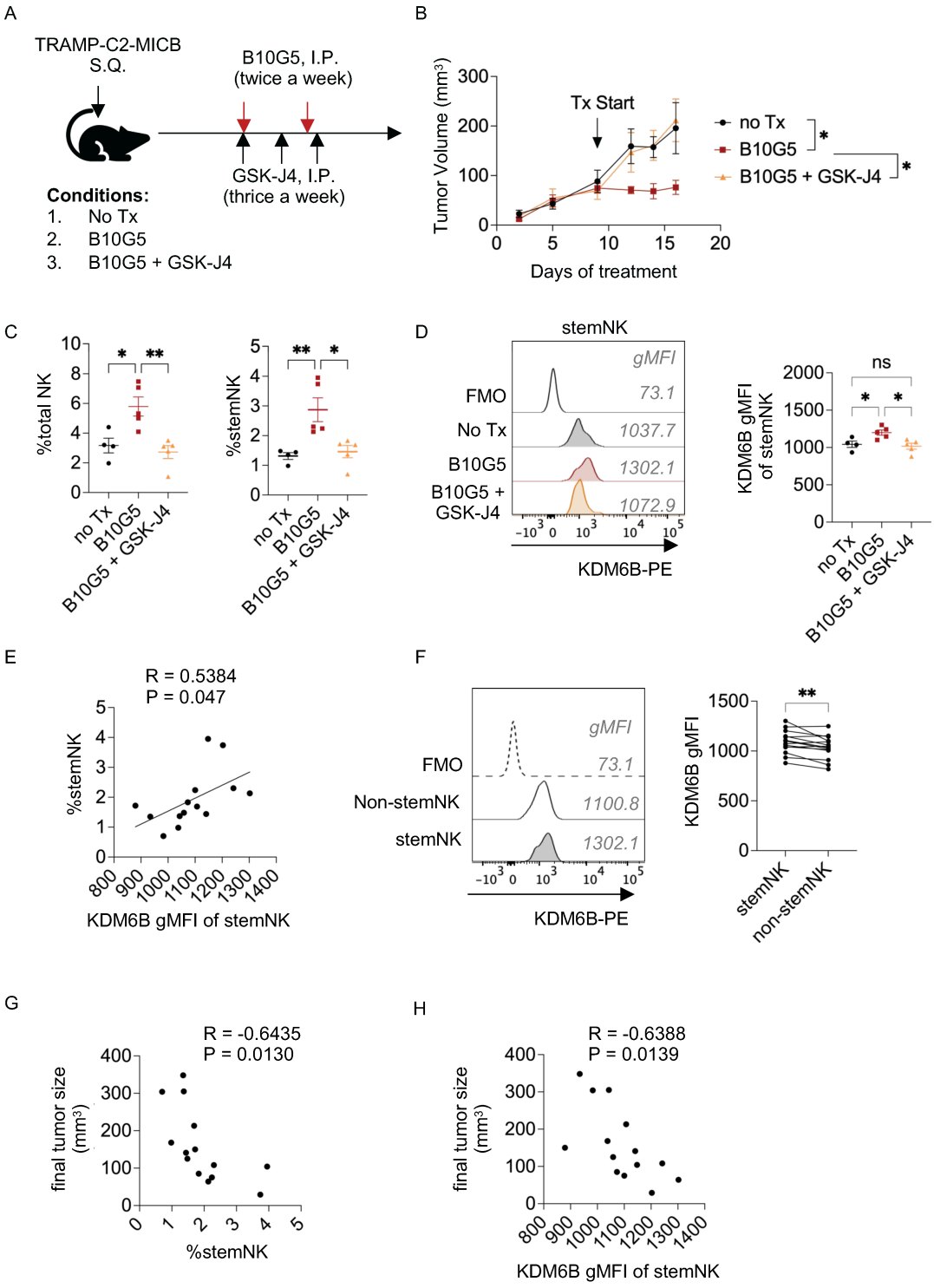

Figure 4. KDM6B demethylase activity is required for maintenance of stemNK cells.

(A) Mice bearing TRAMP-C2-MICB tumor cells were randomized to treatment groups as indicated (n=4-5/group). B10G5 was administered at 200 ug/mouse via intraperitoneal (IP) injections twice weekly, whereas GSK-J4 (10 mg/kg per mouse) was given IP thrice weekly. (B)

Tumor growth curves. (C) Percentage of total NK and stemNK cells ($CD3^-$ $NK1.1^+EOMES^{hi}TCF1^{hi}$), normalized to total live events. Gating strategy is provided in Supplemental Figure 8. (D) KDM6B expression (geoMFI) of tumoral stemNK cells. (E) Pearson correlation between KDM6B expression (geoMFI) and stemNK cell enrichment. (F) KDM6B expression (geoMFI) in stemNK and non-stemNK cells. (G-H) Pearson correlation between final tumor volume (mm^3) and percentage (G) or KDM6B expression (gMFI) (H) in stemNK cells. Statistical analyses were performed using repeated measure two-way ANOVA with the Geisser-Greenhouse correction (B), one-way ANOVA with Tukey's multiple comparison tests (C-D), and paired t-test (F). Data were shown as mean +/- SEM. *$p < 0.05$, **$p < 0.01$, ***$p < 0.001$.

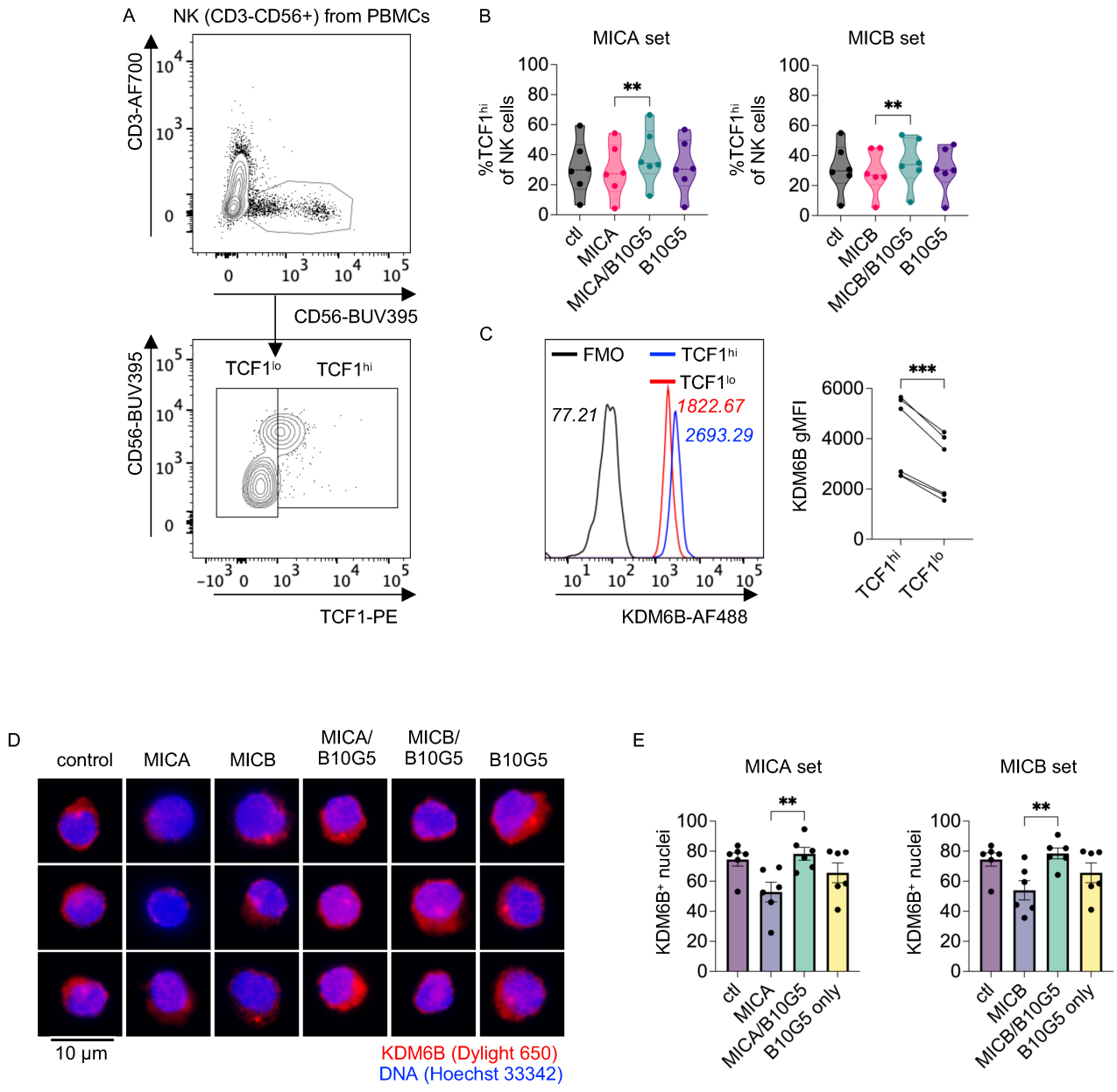

Figure 5. Attenuating NKG2D stimulation upregulates KDM6B and TCF1 expression in human NK cells.

(A-B) Health donor PBMCs were cultured with sMIC only, pre-formed sMIC/B10G5 complex, B10G5 only, or PBS for 24 hours. TCF1^{hi} NK were quantified by flow cytometry among CD3^{-} CD56^{+} cells. Each datapoint represents value from one PBMC donor with total six donors. (C) KDM6B expression in TCF1^{hi} and TCF1^{lo} NK cells from PBMCs of six donors. (D) Representative Immunofluorescence staining of KDM6B with Hoechst nuclear counterstain for primary human

NK cells stimulated as indicated for 5 days in vitro. 63 x magnification. Scale bar, 10 µm. (E) Average %KDM6B^{+} nuclei from 6 donors for MICA and MICB respectively. Each datapoint represents value from one experiment. Statistical analyses were performed using Friedman tests with Dunn's multiple comparisons tests (B, E), and paired t-test (C). *$p < 0.05$, **$p < 0.01$, ***$p < 0.001$.

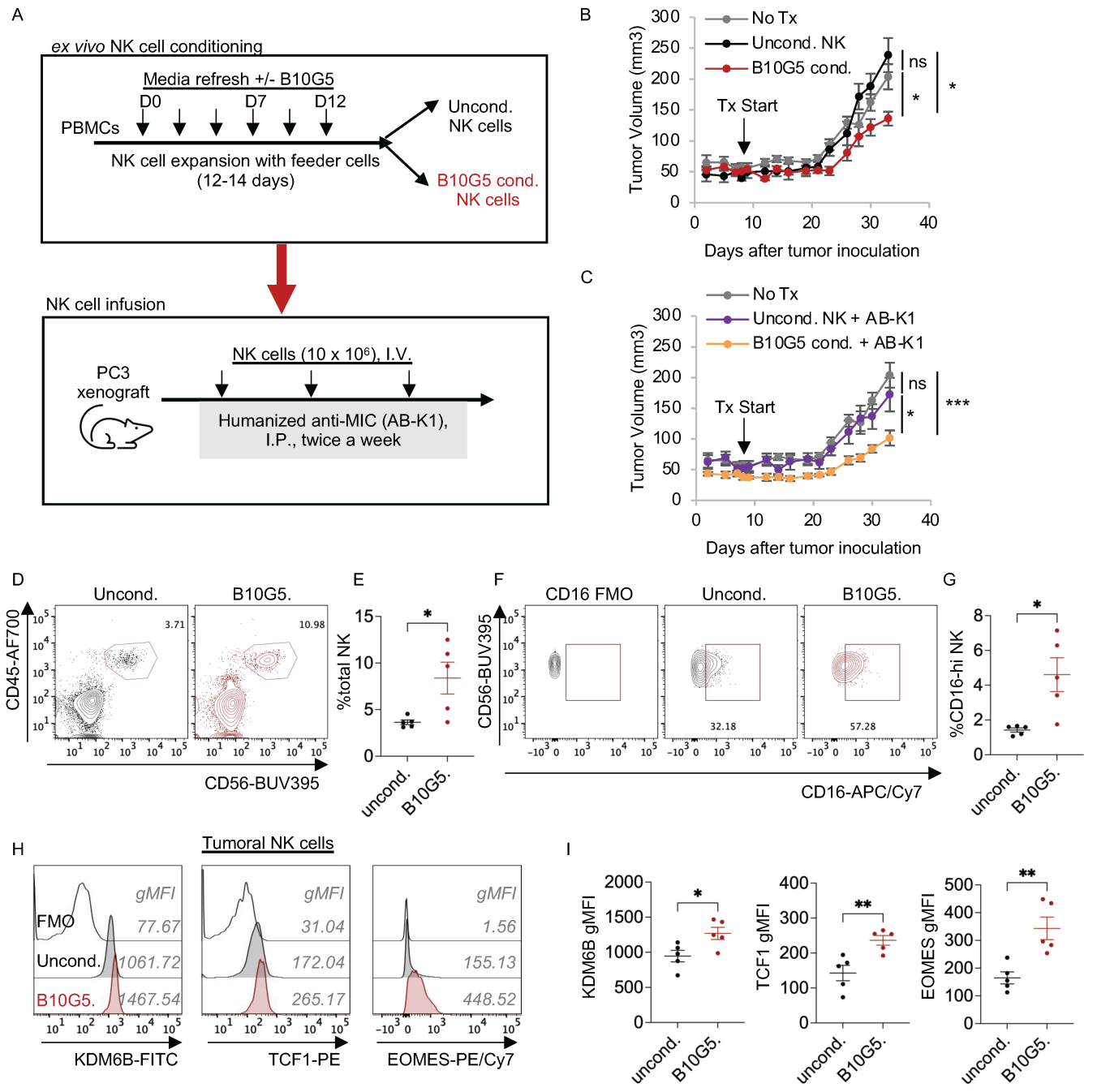

Figure 6. Attenuating NKG2D stimulation during ex vivo expansion enhances NK cell in vivo persistence and anti-tumor efficacy.

(A) Human NK cells were expanded from PBMCs co-cultured with MIC^{+} K562-CI9-mIL21 feeder cells pre-incubated with or without B10G5 (1 ug/mL). NCG mice bearing PC3 human prostate

tumors were randomized into 5 treatment groups as indicated (n = 4-7/group). (B-C) Tumor growth curve in each treatment group. (D-E) Percentage of tumoral NK cells (normalized to total live events). (F-G) Percentage of tumoral $CD16^{hi}$ NK cells (normalized to total live events). (H-I) KDM6B, TCF1 and EOMES expression in tumoral NK cells, measured by flow cytometry. Statistical analyses were performed using repeated measure (RM) two-way ANOVA with the Geisser-Greenhouse correction (B-C) and Welch's t-tests (E, G, I). $*p < 0.05$, $**p < 0.01$, $***p < 0.001$.

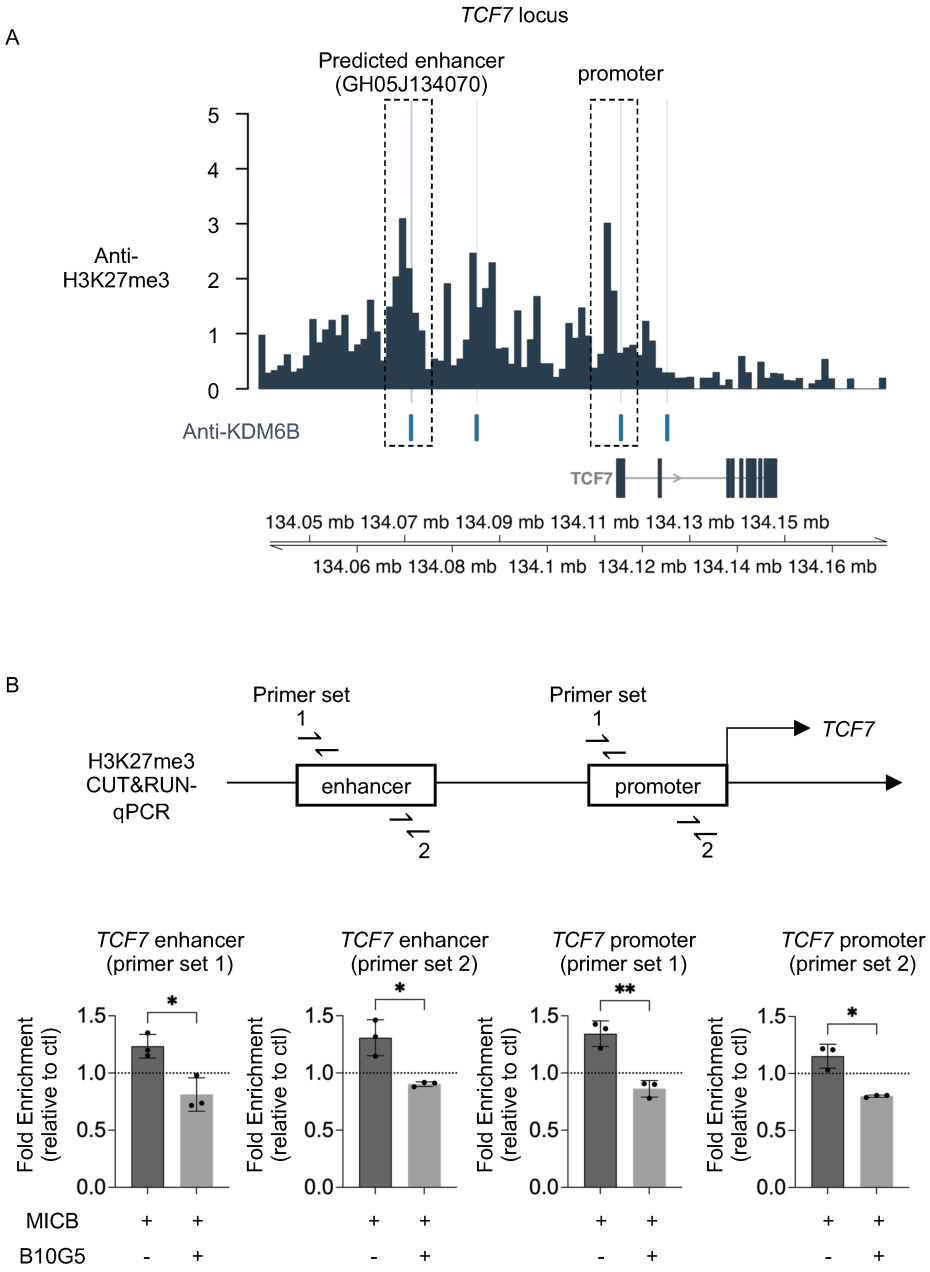

995

996 **Figure 7: Attenuating NKG2D stimulation decreases H3K27me3 at the *TCF7* locus.**

997 (A) Coverage plot of anti-H3K27me3 binding (GSE209425) at human *TCF7* (encoding TCF1)
998 gene locus, which aligned with predicted KDM6B binding sites obtained from ChIP-Atlas. (B)
999 H3K27me3 enrichment at *TCF7* promoter and enhancer regions, measured with CUT&RUN-
1000 qPCR of primary human NK cells stimulated with sMIC or B10G5/sMIC complex for 5 days (n =

3). Relative enrichment (%input) was normalized to unstimulated vehicle control samples. Statistical analyses were performed using Welch's t-tests (B). *$p < 0.05$, **$p < 0.01$, ***$p < 0.001$.